ENCAPSULATION OF FERULIC ACID WITH HYDROXYPROPYL METHYLCELLULOSE AND XANTHAN GUM BIOPOLYMERIC SYSTEMS

ZAW MYO HTET

MASTER OF SCIENCE
IN
CREATIVE INNOVATION IN COSMETIC SCIENCE

SCHOOL OF COSMETIC SCIENCE
MAE FAH LUANG UNIVERSITY

2025

ENCAPSULATION OF FERULIC ACID WITH HYDROXYPROPYL METHYLCELLULOSE AND XANTHAN GUM BIOPOLYMERIC SYSTEMS

ZAW MYO HTET

THIS THESIS IS A PARTIAL FULFILLMENT OF
THE REQUIREMENTS FOR THE DEGREE OF
MASTER OF SCIENCE
IN
CREATIVE INNOVATION IN COSMETIC SCIENCE

SCHOOL OF COSMETIC SCIENCE
MAE FAH LUANG UNIVERSITY
2025

THESIS APPROVAL

MAE FAH LUANG UNIVERSITY

FOR

MASTER OF SCIENCE

IN

CREATIVE INNOVATION IN COSMETIC SCIENCE

Thesis Title: Encapsulation of Ferulic Acid with Hydroxypropyl Methylcellulose and Xanthan Gum Biopolymeric Systems

Author: Zaw Myo Htet

Examination Committee:

Associate Professor Mayuree Kanlayavattanakul, Ph. D.	Chairperson
Associate Professor Nattaya Lourith, Ph. D.	Member
Associate Professor Chaisak Chansriniyom, Ph. D.	Member

Advisor:

.....Advisor

(Associate Professor Nattaya Lourith, Ph. D.)

Dean:

.....

(Associate Professor Wandee Rungseevijitprapa, Ph. D.)

ACKNOWLEDGEMENTS

First and foremost, I would like to express my sincere gratitude to my advisor, Assoc. Prof. Dr. Nattaya Lourith for her invaluable suggestion, insightful feedback, continuous encouragement, and kind supervision throughout this research study.

I am truly grateful to my thesis defense committee members, Assoc. Prof. Dr. Mayuree Kanlayavattanakul, and Assoc. Prof. Dr. Chaisak Chansriniyom for their expertise, insightful comments and knowledge contributions to my research work.

Moreover, special thanks to staff members from School of Cosmetic Science, and Office of Postgraduate Studies, MFU for their assistance and financial support in enabling research facilities and conference proceeding grants.

Furthermore, my thanks are extended to my family, colleagues and friends from Creative Innovation in Cosmetic Science graduate program for their moral support and encouragement in any part of the thesis study.

Finally, I genuinely appreciate European Union Mobility Programme for Myanmar (EMPM) for their full scholarship support during my entire master's degree journey at Mae Fah Luang University.

Zaw Myo Htet

Thesis Title	Encapsulation of Ferulic Acid with Hydroxypropyl Methylcellulose and Xanthan Gum Biopolymeric Systems
Author	Zaw Myo Htet
Degree	Master of Science (Creative Innovation in Cosmetic Science)
Advisor	Associate Professor Nattaya Lourith, Ph. D.

ABSTRACT

Ferulic acid (FA) is a phenolic antioxidant widely used in cosmetics due to its pharmacological properties. Nonetheless, its stability detriments its applications abided by the formulating practices and its bioavailability. This study aimed to develop biopolymeric walls using hydroxypropyl methylcellulose (HPMC) and xanthan gum (XG) for FA encapsulation. The biopolymeric walls with HPMC and XG (50:1 to 250:1 w/w) afforded the amorphous particles with pore sizes of 37-51 μm as demonstrated with SEM and ImageJ calculation and showed moderate lightness (44.26-46.25), a* (0.08-0.16), and b* (5.24-6.43). FTIR confirmed the bonding between HPMC and XG through characteristic O–H, C=O, and C–O–C bands. DSC and XRD improved thermal behavior and amorphous structure. FA was loaded (1.22–1.23% w/w) with the encapsulation efficiencies of 71.26–80.52%. Encapsulation reduced yellowness (b*) from 15.80 ± 0.07 to 9.23 ± 0.09, while SEM, FTIR, DSC, and XRD further confirmed FA encapsulation. Physicochemical properties showed the water solubility increasing from 30–38% to 34–40%, the water absorption rate from 16–18% to 17–25%, and the swelling capacity from 4×10^{-3} to 7×10^{-3} %. Controlled release showed an initial slow FA release of 14.66–25.31% in the first 6 h reaching 37.97–49.07% at 72 h. Under accelerated stability testing (40°C and 75 % RH), encapsulation efficiency dropped to 48.82–62.88% with increased b* 10.27 ± 0.06 to 28.6 ± 0.01, while the formulation containing 0.05 g XG and FA added before hydration proved superior in FA retention.

Keywords: Ferulic Acid, Biopolymeric Walls, Encapsulation, Cosmetics

TABLE OF CONTENTS

TABLE OF CONTENTS

LIST OF TABLES

LIST OF FIGURES

ABBREVIATIONS AND SYMBOLS

FA	Ferulic acid
SPF	Sun protection factor
PF	Protection factor
UVA-PF	Ultraviolet A protection factor
MD	Maltodextrin
HPMC	Hydroxypropyl methylcellulose
XG	Xanthan gum
SEM	Scanning electron microscope
TEM	Transmission electron microscopy
FTIR	Fourier transform infrared spectroscopy
ATR	Attenuated total reflectance
DSC	Differential scanning calorimetry
XRD	X-ray diffraction
WSI	Water solubility index
WAR	Water absorption rate
SC	Swelling capacity
HPLC	High performance liquid chromatography
UV-Vis	Ultraviolet Visible Spectroscopy
EE	Encapsulation efficiency
PBS	Phosphate-buffered saline
ICH	International Council for Harmonisation of Technical Requirements for Pharmaceuticals for Human Use
RH	Relative humidity

CHAPTER 1

INTRODUCTION

1.1 Background of the Study

Antioxidants are the popular actives used in skincare products, and they were shown being effective to prevent skin aging caused by intrinsic and extrinsic conditions (Vierkötter & Krutmann, 2012). Ferulic acid (FA), 4-hydroxy-3-methoxycinnamic acid is a phenolic compound with potent antioxidants, anti-inflammatory and anti-aging properties showing its high potent to be used in face masks and moisturizing creams at a recommended concentration 0.5% to 1% (Purushothaman & Rizwanullah, 2024; Zduńska et al., 2018). When applied topically, FA shows photoprotective effects, reduces hyperpigmentation, improves skin elasticity, and enhances overall skin texture (Purushothaman & Rizwanullah, 2024). FA neutralizes reactive oxygen species such as hydroxyl radicals and superoxide anions to protect skin cells from oxidative damage. FA (0.5%) stabilizes the efficacy of 15% Vitamin C and 1% Vitamin E. Combined; this antioxidant triad provides 8 times greater photoprotection than 4-fold of Vitamin C and E. FA (1% w/w) reaches the sun protection factor (SPF) 26 and UVA protection factor (UVA-PF) 14 when mixed with other UV filters (Lin et al., 2005).

Despite its promising therapeutic and biological activities, FA faces stability challenges that limit cosmetic applications which affect reduction of FA concentration and color changes over time. FA's poor chemical stability remains the biggest challenge especially at basic pH, high temperature, long exposure to light, and in the pair use with incompatible ingredients (Gupta et al., 2020). Additionally, when FA was added in skincare formulations, it tends to show poor skin permeation, limiting its use in topical formulations. Previous study reported that free FA retained only 50% after one month exposure at high temperature (45°C) and relative humidity (80% RH) while FA dropped to approximately 35% under fluorescent light at room temperature (Pueknang & Saewan, 2022). Another study reported FA dropped to approximately 60% after 24 h UVB irradiation. This event of rapid degradation impairs the shelf life and efficacy of FA containing products, showing the need for better formulations to improve FA

stability. Although there are numerous methods to prolong FA stability, encapsulation is perceived with greater attention for protecting the active against degradation, enhancing stability and controlling the release of actives (Mitura et al., 2020).

In recent years, natural and synthetic polymers are introduced as wall materials or carrier systems that use polysaccharides (alginate, chitosan, starch, cellulose derivatives), and proteins (gelatin, whey protein, zein) which can swell, dissolve, or break down on specific skin conditions. Hydroxypropyl methylcellulose (HPMC) is a hydrophilic, semi-synthetic cellulose derivative recognized for its high film forming ability creating a barrier around active compounds by reducing oxygen and moisture permeability. HPMC based encapsulation system enabled maximum encapsulation efficiency of 85.56% at a ratio of FA 10%: HPMC 25% (Yu et al., 2021). Xanthan gum (XG), an anionic natural polysaccharide produced by the bacterium *Xanthomonas campestris* contributes rapid hydration, high viscosity at low concentrations and heat stability properties. Its high molecular weight and rheological properties are suitable to be used as stabilizing agent for water-based systems (Chaturvedi et al., 2021). Using biopolymer blends are more effective in improving the stability of the phenolics, particularly FA because the blended system can improve water solubility in aqueous environments exemplified by FA's hydrophobicity necessitating biopolymer walls that can enhance solubility (Sweed et al., 2024). A previous study showed that the use of biopolymer blends can enhance encapsulation performance, reporting high encapsulation efficiencies of 98.33% for maltodextrin (MD) alone, 97.71% for MD and carboxymethyl cellulose, 98.09% for MD and gum Arabic, and 93.75% for MD and XG (Jang & Koh, 2023). At present, there are insufficient studies on cosmetic oriented biopolymer systems for FA delivery using synthetic, modified derivatives, and natural, microbial polysaccharides namely XG. Following a review of previous studies for FA encapsulation, the combination of HPMC and XG for this research is believed to be a complementary wall system to overcome individual polymer limitations, enhance encapsulation efficiency and achieve releasing kinetics.

1.2 Objectives of the Study

1.2.1 To prepare and characterize the developed biopolymeric walls composing of either a blend of HPMC and XG or HPMC only

1.2.2 To prepare and characterize the encapsulated FA in the developed biopolymeric walls

1.2.3 To determine encapsulation efficiency of FA in the walls

1.2.4 To evaluate controlled release and stability of the encapsulated FA

1.3 Scope of the Study

1.3.1 Preparation of biopolymeric walls

Biopolymeric walls with four concentrations were prepared using 2.5 g of HPMC and different quantity of XG (0.05, 0.02, 0.01 g) or without XG. Characterization of the walls was undertaken by visual assessment, color analysis by colorimeter, scanning electron microscopy (SEM), Fourier-transform infrared spectroscopy (attenuated total reflectance), differential scanning colorimetry (DSC), X-Ray diffraction (XRD). Physicochemical properties were determined in terms of water solubility index, water absorption rate, and swelling capacity.

1.3.2 Preparation of encapsulated FA

Encapsulated FA was prepared by loading FA at a concentration of 1.22–1.23% w/w to biopolymeric walls via freeze drying. FA encapsulated were determined in terms of encapsulation efficiency and its characterization were assessed by visual assessment, color analysis, SEM, FTIR, DSC, and XRD. The same physicochemical properties and controlled release were evaluated. Stability of FA encapsulated systems was monitored in duration of 6 months under the conditions, 40 ± 2°C and relative humidity 75 ± 5% followed by reassessment of color and encapsulation efficiency at different time interval. Photostability was assessed in climatic chamber at 25°C ± 2°C for 7 days by adjusting the distance between the bottom of the vial and the light.

1.4 Output of the Study

The primary output of this study is the understanding of biopolymeric wall systems using dual (HPMC and XG) and single polymer (HPMC) for FA encapsulation. The study provides scientific evidence regarding the influence of polymer composition on physicochemical characteristics, encapsulation performance, release behavior, and stability of FA-loaded systems. Furthermore, it identifies the appropriate biopolymeric wall composition for improving FA stability and delivery potential in topical and cosmetic applications, thereby contributing to the development of more optimized biopolymeric encapsulation systems for cosmetic formulations.

CHAPTER 2

LITERATURE REVIEWS

2.1 Ferulic Acid

Ferulic acid (FA) is a phytochemical phenolic compound found in several plant species such as eggplants, cabbage, bananas, spinach, garlic chives and grains. FA is a hydroxycinnamic acid with a molecular formula of $C_{10}H_{10}O_4$ and molecular weight of 194.18 g/mol as well as melting point in the range 168-172°C (Purushothaman & Rizwanullah, 2024). In cosmetic industries, it is used for its antioxidants, soothing, brightening and UV protection properties and used in serum, lotions, and creams to prevent skin aging, and to look skin brighter and smoother. FA was shown to improve the stability and efficacy of other antioxidants of vitamin C and E, making it potent in developing multifunctional cosmetic formulations.

However, the instability of FA and its susceptibility to rapid degradation by light, heat and oxidation limits its efficacy in topical formulations (Shukla et al., 2022). Furthermore, FA's poor solubility and limited bioavailability inhibit penetration into the skin layers. FA was described as its low water solubility (<1µg/mL) due to the presence of benzene ring and the carbonic side chain in its structure, leading to challenges in cosmetic formulations (Cavalcanti et al., 2020). Photostability studies showed that free FA dropped to approximately 70% after 20 h of UVB irradiation and 60% after 24 h exposure (Yu et al., 2021). This degradation compromises its therapeutic potential and poses a challenge to optimize full benefits. Additionally, FA's poor skin permeability leads to precipitation and deposition in crystallized form and therefore cannot be delivered to skin, affecting its therapeutic efficacy. These limitations show the necessity for advanced delivery systems for FA to enhance solubility, improve stability and promote skin penetration in cosmetic and dermatological applications.

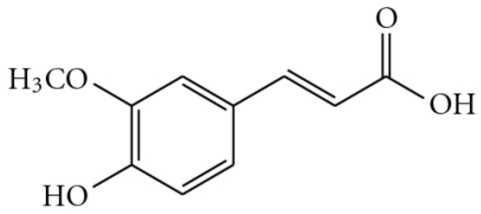

Source Lin et al. (2012)

Figure 2.1 Ferulic acid structure

2.2 Encapsulation

Encapsulation is one of the advanced delivery techniques to improve thermo-sensitive actives' stability, solubility and delivery, particularly using biopolymeric walls. Encapsulation is vital for benefiting controlled release, enhancing its dermal penetration, and maximizing therapeutic efficacy in cosmetic preparations (Velázquez, 2025). Delivery systems are critical in cosmetic formulations nowadays because topical application necessitates the delivery of actives through the skin's lipid barrier to desired layers. Advanced delivery systems offer key benefits by maintaining therapeutic levels of actives over extended period, delivering actives specifically to desired areas, lowering the required dose, and reducing exposure to non-target tissues. Despite these benefits, the development of such delivery systems lacks precise release kinetics and may reduce the bioactivity if the release kinetics is not optimal (Kouassi et al., 2022).

Encapsulation is a type of delivery system where actives are enclosed within a wall material to form particles or capsules. Encapsulation has great potential for delivering some sensitive actives under carefully controlled systems, e.g. alpha hydroxy acids, glycolic acid, salicylic acid, peptides, silicone emulsions (Casanova & Santos, 2016). Encapsulation offers improved solubility, enhanced stability, controlled release, and targeted delivery; by contrast, scale-up issues, cost and complexity along with potential interactions with wall materials are great concerns. The role of wall materials plays an important role in evaluating encapsulation efficiency only if they have adequate rheological properties and are compatible with active ingredients for industrial applications (Akpo et al., 2024). Selecting wall materials depends on various factors

such as viscosity, toxicity, particle size, release of actives from the vehicle, and rate of penetration into the stratum corneum.

Different methods are available for encapsulation of phenolic compounds, among which spray drying, freeze drying, coacervation, and ionic gelation are the popular methods. Spray drying is guided by the injection of solution in atomizing nozzle, and release in the form of droplets from a close chamber circulating with hot air, giving higher encapsulation efficiency in a short time, yet this technology can affect thermal sensitive phenolics and challenge to control particle size (Mudalip et al., 2019). Coacervation originates from the concept of separation into two phases via interaction of oppositely charged ions, but it has disadvantages of high storage cost, complex process control, poor active loading, and limited stability (Costa et al., 2020). Ionic gelation is processed by means of dropping solution into ionic solution under constant agitation, but it shows poor stability in acidic pH and not appropriate for high molecular weight compounds (Ozkan et al., 2019). Freeze drying (lyophilization) is ideal for encapsulating heat sensitive actives by removing solvents at low temperatures and vacuum pressure, resulting in improved solubility and exceptional stability due to the porous structure of freeze-dried products despite it is time consuming (Rezvankhah et al., 2020). Biopolymers are widely used as wall materials in encapsulation systems due to their ability to protect sensitive bioactive phenolic compounds while enabling controlled release. They are often preferred in encapsulation systems due to their biodegradability, low toxicity and bioavailability.

2.2.1 Hydroxypropyl methylcellulose

Hydroxypropyl methylcellulose (HPMC) is a propylene glycol of methyl cellulose ether which is hydrophilic polymer used in skin delivery systems. It was derived from natural cellulose via esterification process, where hydroxyl groups in its original structure are substituted with hydroxypropyl and methyl groups (Yu et al., 2023). When HPMC is dissolved in water, cellulose ethers quickly hydrate and swell, creating a gel layer that is influenced by its hydrophilic hydroxypropyl and hydrophobic methoxy substituent levels. Dispersion of HPMC enables hydrogen bonds due to the presence of polar and nonpolar side groups in its structure (Yu et al., 2021). HPMC has different viscosity levels range from 3 to 100,000 mPa·s measured in 2% aqueous solution (w/w) at 20°C from which low viscosity is for film coating solutions with

aqueous solvents, whereas high viscosity is used in organic solvents. HPMC is popular across cosmetic industry due to its several properties including solubility and gelling behavior, rheological modifier, film formation and water retention. HPMC provides important functional roles in cosmetic formulations by not only yielding a uniform gel-like texture suitable for sensitive skin types but also enhancing stability of cosmetic formulations containing retinol, niacinamide or hyaluronic acid. More importantly, it contributes to sustained release of salicylic acid, botanical extracts or zinc pyrrolidone carboxylic acid that further boosts the efficacy of those active ingredients (Vlad et al., 2025). HPMC remains as environmentally friendly versatile polymer that presents its benefits in vegan, animal free cosmeceutical and nutraceutical products.

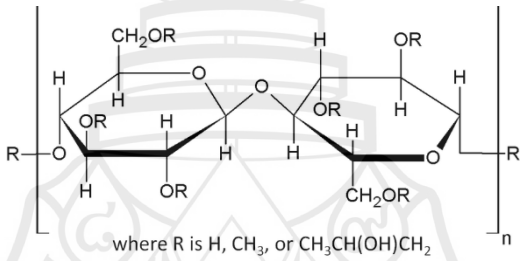

Source Quinten et al. (2021)

Figure 2.2 Hydroxypropyl methylcellulose structure

2.2.2 Xanthan gum

Xanthan gum (XG) is a white to cream-colored fine powder with colorless, tasteless, and odorless characteristics and produced by the bacterium *Xanthomonas campestris*. Its low viscosity works at high shear rates while high viscosity does at low shear rates. XG shows high stability against thermal, acidic, and alkaline conditions and its thermal stability is higher than other water-soluble hydrocolloids (Cai et al., 2019). It is a hydrophilic polymer with its polyelectrolyte nature being soluble in both cold and hot water. Due to its exceptional properties as stabilizer and thickener, XG is used in foods, personal care, cosmetics and toiletries (Dave & Gor, 2018). It has molecular weight in the range 2×10^6 to 2×10^7 g/mol showing better thermal stability than other polysaccharides, and its viscosity is not affected by heat application (Mendoza-Muñoz et al., 2023). Its high molecular weight favors the formation of physical and chemical networks to improve the stability of the carrier (Yadav & Karthikeyan, 2019).

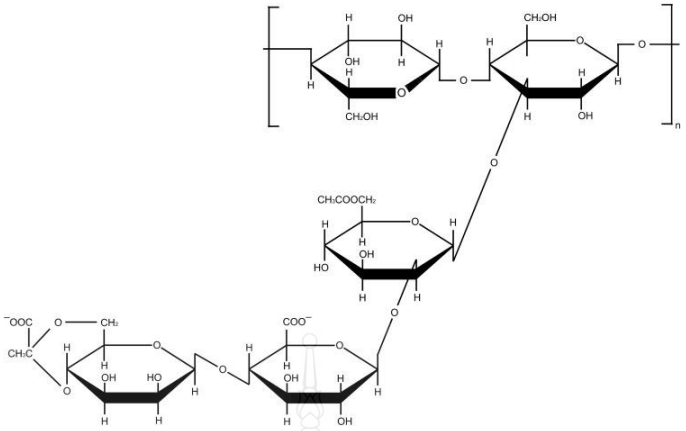

Source Krstonošić et al. (2021)

Figure 2.3 Xanthan gum structure

2.3 Characterization

The characterization of biopolymeric walls and FA-loaded systems is critical for developing stable cosmetic formulations. Comprehensive characterization involves analysis of molecular structure, morphology, thermal behavior, crystallinity, and the presence of incorporated active substances. Key analytical techniques—such as color analysis, scanning electron microscopy (SEM), Fourier-transform infrared spectroscopy (FTIR), differential scanning calorimetry (DSC), and X-ray diffraction (XRD) are used to determine surface morphology, chemical bonding, thermal behavior, and crystalline/amorphous states of encapsulated FA, all of which have great influences on the physicochemical properties, release profile and stability of encapsulated cosmetic ingredients (Yang et al., 2020). For FA-loaded biopolymeric systems intended for cosmetic applications, characterization focuses on confirming successful encapsulation, FA–polymer interactions and ensuring structural and thermal stability.

2.3.1 Color analysis

Visual observation and subjective assessment often lack precision with respect to informing color values. The visually observed color of an object depends on (1) the type of illuminating light, (2) light modification by interaction with the object, and (3) the characteristics of the observer response (Weatherall & Coombs, 1992). The International Commission on Illumination, known as CIE, introduced CIELAB in 1976,

a three-dimensional color space consisting of three axes; L* indicates lightness whereas a* and b* show chromaticity coordinates. CIELAB is a common system for quantitative color measurement of an object and useful in scientific research and clinical studies due to its uniformity, ease of acquisition, and device independence (Afonso et al., 2017).

The color values are often measured using a colorimeter which precisely measures the primary values of L*a*b* in which L* measures white to black (lower L* for dark color while higher L* for white, light color), a* shows redness and greenness (positive a* hints red, and negative a* expresses green), and b* demonstrates yellow by positive and blue by negative values respectively. A previous study reported that formulations with HPMC and XG exhibited L* = 65 ± 2, a* = 1.1 ± 0.3, and b* = 11.5 ± 0.9, indicating a slightly yellowish crumb with moderate lightness (Torres-Perez et al., 2023). Another study using encapsulated gel formulations revealed FA retained 95% of initial luminosity (L*= 89.2) after 90 days, while free FA showed 40% reduction in L*, changing to amber color (Das & Wong, 2020). The CIELAB color is more advantageous than tristimulus values due to its conceptual alignment with the visual experience of color, and it offers a benefit by enabling the quantification of differences between any two colors.

2.3.2 Morphology

Morphology studies refer to internal and external structure, shape, size and surface of the materials which largely depend on the operating conditions that are used to produce the microcapsules and the wall materials used. Morphology analytical techniques include microscopy, thermal analysis, dynamic light scattering and interferometry. Recent advances used in the high-resolution transmission electron microscopes and interpreting the images, have allowed resolutions of the order of atomic structures in inorganic crystal.

Electron microscopy (EM) can be divided into the techniques of transmission electron microscopy (TEM) and scanning electron microscopy (SEM). SEM uses electron beams, but unlike TEM, which requires extremely thin specimens, SEM can image thicker samples, making it useful for determining bulk materials. SEM is the most popular of microscopic techniques, due to the user-friendliness of the apparatus, the ease of specimen preparation, and the general simplicity of image interpretation (Guo, 2016). SEM has been widely used for decades in the study and analysis of

biopolymer systems to gain information pertaining to the structure, morphology, size, shape, surface modifications, wear and tear, etc (Venkateshaiah et al., 2020). The applications are found in polymorphism studies, particle size analysis, surface roughness & structure, internal & external morphology. HPMC-XG composite films displayed a smooth, continuous surface with homogeneous polymer blending, attributed to hydrogen bonding between XG's carboxyl groups and HPMC's hydroxyl residues (Zheng et al., 2022). A study of Yu et al. (2021) revealed that encapsulated FA formed amorphous aggregates whereas free FA showed needle-like crystals.

2.3.3 Fourier-transform infrared spectroscopy

Fourier-transform infrared spectroscopy (FTIR) works on the principle that molecules absorb infrared light at specific frequencies, which correspond to the vibrational modes of their chemical bonds. FTIR analysis can prove the presence of specific functional groups and help confirm the encapsulation of compounds within the microcapsules. FTIR spectroscopy has two main sampling techniques which are transmission and attenuated total reflectance (ATR) whereas ATR has attracted more attention for characterization due to its access to the surface vibrational frequencies, as opposed to bulk material. ATR measures the absorption of infrared light by a sample placed in close contact with a high refractive index crystal (Patkowska et al., 2025).

Due to the presence of hydroxypropyl and methyl groups in HPMC, the bands at 3400 and 1050 cm^{-1} can confirm the substitution of hydroxyl groups in the cellulose backbone with methoxy and hydroxypropyl groups, distinguishing HPMC from native cellulose (Schantz et al., 2014). XG is composed of a cellulose backbone with trisaccharide side chains, so it shares common structural features with HPMC as their distinct bands corresponding to carbonyl groups underscore their unique modification. XG spectra exhibit characteristic peaks at 1,610 cm^{-1} (C=O stretching of acetyl groups) and 1,410 cm^{-1} (–CH_2 scissoring), while HPMC shows O–H stretching at 3,450 cm^{-1} and C–O–C vibrations at 1,050 cm^{-1} (Sowmya et al., 2022).Characteristic peaks of FA were found at 1619, 1,514 cm^{-1} showing C=C aromatic ring, and 1,272, 1,205 cm^{-1} indicated the presence of C-H bending (Venkateswarlu, 2017). Stable encapsulation alters FA's peaks due to molecular interactions with the wall material. Encapsulated FA lost FA's characteristic hydroxyl (3436 cm^{-1}) and carbonyl (1619 cm^{-1}) peaks, showing a new interaction peak at 1688 cm^{-1} (Pueknang & Saewan, 2022).

2.3.4 Differential Scanning Colorimetry

Differential scanning colorimetry is a method of thermal analysis used to determine thermal transitions, i.e., solid-solid transitions or solid liquid and other transitions. Thermal analysis can determine rapidly and accurately the transformation of crystal material type, melting, sublimation, dehydration, absorption, and decomposition of changes, is an important method to determine the physical and chemical properties of inorganic, organic and polymer materials (Wang et al., 2018). Amorphous polymers exhibit glass transition temperature, and semi-crystalline polymers possess crystallization temperature and melting temperature with various crystallization and melting enthalpies (Adriana, 2013). HPMC displays a broad endotherm at 60–140°C, corresponding to moisture loss, however, the precise temperature depends on the integrity of the seal of the pan (Ford, 1999). XG showed an exothermic peak at 285.8°C representing thermal degradation or decomposition due to elevated temperatures. A study of Sajjadi et al. (2012) showed FA's sharp peak at 168°C (ΔH = 142 J/g) corresponding to crystalline FA representing melting endotherm. DSC is used for many industrial applications which include finding polymorphic transitions, melting points, glass transition state, thermal processing conditions, crystallization temperature, thermal safety/stability, effect of additives, polymer blends, degree of cure, and protein denaturation (Lukas & LeMaire, 2009). Improvement of the thermal stability in terms of change of thermal degradation temperature by DSC, together with the results of chemical bonding (e.g. FTIR), can indicate successful encapsulation in polymeric wall systems (Yang et al., 2020).

2.3.5 X-Ray diffraction

X-Ray diffraction is used to determine the crystallinity and nature of solid particles, whereas crystallinity is defined as the mass fraction of the crystalline regions in a material. For example, the higher the crystallinity of a polymer, the more properly the chains of that polymer are aligned. Crystallinity has an important effect on many physical and chemical properties of polymers. The higher the crystallinity of a polymer, the higher the hardness and density of that polymer. HPMC is a semi-synthetic derivative of cellulose, exhibiting amorphous structure due to the introduction of hydroxypropyl and methyl groups disrupting the native crystalline cellulose framework while XG is well known for its predominantly amorphous character, evidenced by

broad, diffuse peaks in its diffraction pattern (Noorlaila et al., 2017). A study of Yu et al. (2021) reported the presence of crystalline structure in FA in which distinct, sharp peaks correspond to its molecular arrangement. FA demonstrates crystalline peaks at 12.8°, 16.4° and 22.7°. HPMC is semi-crystalline, with diffraction peaks at 8.6° and 20.1°, while crude XG shows diffractogram with one crystalline peak at 22.30° (Zheng et al., 2022).

2.4 Physicochemical Properties of Biopolymeric Walls and Encapsulation Systems

FA is poorly soluble in water at acidic to neutral pH, however, cosmetic products are usually formulated near skin pH (4.5-6.0) in which FA remains insoluble (Das & Wong, 2020). This limits FA loading or usage in water-based formulations and leads to instability over shelf life. Such defects, limited solubility at skin-friendly pH, susceptibility to oxidation and light are the main barriers to FA direct incorporation in topical products. Biopolymeric walls create protective environments for FA, where the water solubility index, water absorption rate, and swelling capacity are considered to ensure cosmetic formulation stability. The walls with these properties are expected to withstand premature dissolution in aqueous cosmetic bases while maintaining FA release upon application. Biopolymeric wall materials enhance the apparent solubility and uniform dispersion of FA, modulate FA release, improve its photoprotective properties in topical products, and improve the physical stability, texture and sensory attributes to use in cosmetic products.

Water solubility index (WSI) measures the proportion of soluble components released from a material when dispersed in water. Encapsulating FA in biopolymeric wall with an adequate WSI allows the formation of water-dispersible particles and enables incorporation of encapsulated FA into different cosmetic formulations. WSI is important because it can influence how easily encapsulation can be dispersed in the aqueous phase of topical formulation, affecting the physical stability of the product.

Water absorption rate (WAR) shows the capacity of a substance to absorb and maintain water from their surroundings by forming the gel resistance to release water

during centrifugation (Harasym et al., 2020). WAR indicates initial hydration behavior and can be related to porosity and the presence of hydrophilic groups in the polymer. The initial water uptake tells how quickly water penetrates the wall and reaches FA. Improving WAR allows optimize the physicochemical stability of FA and could potentially modulate its release behavior at the skin surface when exposed to aqueous environments during formulation (Mandal et al., 2025). WAR can be determined by measuring the weight of water absorbed by a known weight of dry substance.

Swelling capacity (SC) refers to the extent to which a substance can expand upon water absorption. Optimizing swelling capacity is important for achieving a controlled release profile, as the degree of hydration directly influences the structural transition of the wall into a gel-like state suitable for active delivery (Bhansali et al., 2021). It is important for polymers and hydrocolloids used in food, pharmaceutic, and cosmetic applications, that affect viscosity, gel formation, and texture. SC is influenced by factors such as molecular structure, cross linking density, temperature and pH conditions (Wang et al., 2023). High swollen polymers such as cellulose derivatives are highly hydrophilic, three-dimensional crosslinked polymeric structures, which can swell in aqueous environment. Studies showed HPMC forms mesoporous structures (10–100 nm) due to its semi-crystalline nature, increases swelling but limits long-term water retention while XG creates microporous networks (<50 nm) stabilized by hydrogen bonding which supports high WAR and SC but reduces solubility (Noorlaila et al., 2017).

2.5 Encapsulation Efficiency

For any encapsulated bioactive, encapsulation efficiency (EE) is the key parameter to inform how much the active is protected, and how much can be delivered. EE represents fraction of the active that is entrapped within the biopolymeric walls. Higher EE is preferred for the purpose of improved protection and stability which remits from less exposure to light, temperature, and oxygen (Palanikumar et al., 2018). EE increases with increasing polymer concentration since high concentration increases the viscosity of solutions by delaying drug diffusion within the polymer droplets.

HPMC's amorphous structure and hydrophilic nature allow it to absorb and retain a significant amount of the active ingredient. The gelation properties of HPMC enable sustained release of the encapsulated compound, improving EE (Deshmukh et al., 2017). XG's carboxyl and hydroxyl groups form hydrogen bonds with HPMC, stabilizing the matrix and improving EE (Ng et al., 2020). The hydrogen bonding between HPMC and XG creates a cohesive network with optimal porosity for encapsulating both hydrophilic and hydrophobic actives while encapsulation using biopolymer blends have claimed high EE for active compounds such as essential oils, herbal extracts and vitamins (Ammala, 2013). UV-Vis spectrophotometry enables the quantification of active compounds within delivery systems by measuring their absorbance at specific wavelengths (Mota et al., 2022). This method allows rapid quantification of FA without the need for complex instrumentation or sample preparation. A study of Pueknang and Saewan (2022) reported that 73% EE was achieved via UV-Vis spectrophotometry at 315 nm by dissolving encapsulated FA in dimethyl sulfoxide. However, another study of Yu et al. (2021) used Sep-Pak experiment with HPLC reporting that EE of FA encapsulated in HPMC was 85% greater than in maltodextrin (80%).

2.6 Controlled Release

For cosmetic applications, the encapsulated substances should be released and absorbed into skin layers before the products are rubbed. However, FA was reported for posing numerous issues, necessitating improved delivery techniques for efficient therapeutic use. FA's low water solubility (less than 1µg/mL) interrupts its absorption and leads to low bioavailability. Controlled release systems are designed to deliver such actives at predetermined time by maintaining concentration while minimizing burst release. Controlled release and encapsulation can protect FA from degradation by pH, light, oxygen and temperature, and especially important for poorly soluble actives whose functional effects (antioxidant, and antimicrobial benefits) improve when exposure is sustained (Petrișor et al., 2023).

In vitro release tests allow formulators to optimize vehicles (e.g. gels, emulsions, capsules) so that FA becomes available at the skin surface. It also enables efficacy evaluation by quantifying how much FA can diffuse out of the product, and stability testing by comparing release profiles before and after storage. These studies provide a correlation between *in vitro* and *in vivo* data, which is essential for the releasing kinetics and therapeutic efficacy of FA in real-world applications (Manian et al., 2022).

There are three common methods for controlled release studies, which are diffusion cells, dialysis method and direct dispersion method. Typical experimental setups use diffusion cells (Franz cells) where a high-performance membrane is chosen to allow free diffusion of FA while blocking particulates or polymers. A study of Pueknang and Saewan (2022) compared the release of FA and encapsulated FA in which the encapsulated FA release rate during the first 10 h was slower than FA's, however, their release rate after 10 h gradually increased. The dialysis method suits FA encapsulated in nanoparticles, liposomes, or polymer matrices when studying controlled-release carriers: FA-loaded nanoparticles (Shen & Burgess, 2013). If FA adsorbs to or is retained by the membrane, release may be artificially slow. The direct dispersion method uses dispersing the sample directly into a release medium, typically an aqueous buffer and is particularly important for assessing the release characteristics and the solubility of the active under controlled conditions (Jayadev & Ismail, 2023). In a direct dispersion method without a membrane, controlled release can be monitored by dispersing the FA-loaded system directly into phosphate buffered saline (PBS), incubating under standardized conditions (pH, temperature, agitation), and periodically sampling the supernatant to quantify the amount of FA that has diffused out. Quantification can be done by UV–Vis spectroscopy or HPLC, as in FA-loaded mesoporous silica and polymeric nanoparticle systems, where cumulative percentage released vs. time curves clearly distinguish fast (70–80% in 6 h) from slower, controlled profiles at 40–60% over 24 h (Romeo et al., 2021). Thus, using direct dispersion in PBS, the importance of controlled release is significant by comparing the FA release from encapsulated systems to free FA, showing how encapsulation slows and facilitates release, improves stability, and can be tailored for specific applications.

2.7 Stability Testing

Chemical stability is vital and imperative for encapsulating cosmetic actives, because loss of stability directly challenges their safety, efficacy, and shelf life and therefore it becomes a quality attribute in cosmetic regulations and industry standards (Min, 2025). Phenolic bioactives are vulnerable to thermal stress, light exposure, oxygen, moisture and pH conditions, which pose oxidation, and photodegradation; this is why stability is considered a “preliminary step” when determining whether an active needs encapsulation. In cosmetics, temperature and light are highly concerned because cosmetic products utilize high temperature during production, transport and storage, and repeated light exposure to the skin surface. Industry-oriented stability assessments challenge cosmetic formulations under accelerated conditions and controlled light exposure, in accordance with the International Council for Harmonization of Technical Requirements for Pharmaceuticals for Human Use (ICH) guidelines that applied for cosmetic industry, to estimate shelf life and ensure that encapsulation capable to improve thermal and photostability of the actives (Casanova & Santos, 2016). Although oxidation remains the main concern, it is often addressed via co-encapsulated antioxidants, whereas thermal and photostability assessments are conducted as practical, industry-scale and are widely used in cosmetic stability testing to prove that encapsulation can sustain active content, color, and bioactivity over time.

FA undergoes thermal degradation via decarboxylation reaction when exposed to high temperature, decomposing into derivatives such as 4-vinyl guaiacol, vanillin, and acetovanillone (Das & Wong, 2020). Stability tests have been attempted to ensure that the cosmetic ingredients or products meet the proposed physical, chemical, biological and efficacy requirements when they are kept under different storage conditions. Accelerated stability testing is usually conducted under high-temperature conditions to accelerate the chemical reactions that may degrade a cosmetic product, predicting how it will behave in the long term. Accelerated stability testing in cosmetics can increase the degradation process of a product by 2 to 3 times for every 10ºC increase in temperature. It is very important for cosmetic products to be photo-stable because they can be exposed to some degrees of light in shop windows, and they can be subject

to direct sunlight or artificial light for long periods of time. Photostability testing is a standard used to evaluate the ability of cosmetic products to maintain their stability and effectiveness when exposed to light. According to Q1B in ICH guideline, the samples should be exposed to 200 W h/m^2 of UVA radiation and 1.2 million lux hours of light (International Council for Harmonization of Technical Requirements for Pharmaceuticals for Human Use [ICH], 1996).

CHAPTER 3

MATERIALS AND METHODS

3.1 Chemicals and Equipment

The following chemicals and laboratory equipments were used in this study, and details of each item are disclosed separately in the lists below.

Table 3.1 List of chemicals

Chemicals	Molecular weight	Company
Ferulic acid	194.18 g/mol	Fisher Scientific, UK
Hydroxypropyl methylcellulose	86,000 g/mol	Sigma, Singapore
Xanthan gum	933.75 g/mol	MySkinRecipes, USA
Ethanol 95%	46.07 g/mol	Chemipan, Thailand
Methanol	32.04 g/mol	Q RëC™, New Zealand

Table 3.2 List of equipments

Equipment	Model	Company
Analytical balance	XT220A	Precisa, Switzerland
Homogenizer	T25 basic	IKA, Germany
Water bath	WTB	Memmert, Germany
pH meter	SevenEasy S20	Mettler Toledo, Switzerland
Shell freezer	7949030	Labconco, USA
Freeze dryer	Beta 1-8 LSCbasic	CHRIST, Germany
Colorimeter	UltraScan	HunterLab, USA
Hot air oven	UNE500	Memmert, Germany
Incubator shaker	SI4-2	Shellab, USA
SEM	MIRA	TESCAN, Czech Republic
FT-IR spectrometer	Nicolet iS50	Thermo Fisher, USA
DSC	DSC 3+	Mettler Toledo, Switzerland

Table 3.2 (continued)

Equipment	Model	Company
X-Ray Diffractrometer	Empyrean	PANalytical, the Netherlands
Ultrasonic bath	690DA	Crest, USA
Refrigerated centrifuge	DL-3020HR	METHER, China
Vortex mixer	Vortex Genie 2™	Scientific Industries, USA
Quartz cuvette	VWR	VWR International, USA
Auto-pipette	Research 1111	Eppendorf, Germany
UV- spectrophotometer	Libra S22	Biochrom, UK
Temperature and humidity chamber	GT-7005-C2X	Gotech, Taiwan
Climatic chamber	KBF P720	Binder, Germany

3.2 Methodology

3.2.1 Preparation of biopolymeric walls

Biopolymeric walls were developed in four different formulations composed of HPMC: XG (50:1 to 250:1 w/w) which were slightly modified based on the optimal XG 0.5% (Jang & Koh, 2023). For biopolymer walls, HPMC was gradually dispersed in reverse osmosis (RO) water in hot water bath at 70°C to ensure complete dispersion, followed by the addition of the corresponding amount of XG (except BW4) at the same conditions, then homogenized at 10,000 rpm for 4 minutes. The mixture was kept at 4°C for 24 h for complete hydration. Thereafter, pH of the gel was measured followed by pre-freezing at –40°C by using a shell freezer and freeze dried for 24 h at a vacuum of less than 1 mbar (Cai et al., 2019). Following the yield percent calculation, the freeze-dried samples were collected and kept in airtight plastic bags.

Table 3.3 Composition of biopolymeric walls

Formula	HPMC (g)	XG (g)	Water (g)	Total weight (g)
BW1	2.5	0.05	70	72.55
BW2	2.5	0.02	70	72.52
BW3	2.5	0.01	70	72.51
BW4	2.5	-	70	72.50

3.2.2 Characterization of biopolymeric walls

3.2.2.1 Visual assessment

Biopolymeric walls were initially checked by the naked eyes of the investigator to visually assess their physical appearances and textures. They were placed on a clean background with a full artificial light with no direct sunlight to ensure consistent lighting. The camera's position was maintained at a constant camera to sample distance of 22 cm by holding the camera parallel to the sample surface to prevent distortion. Three consecutive images were taken for each sample to ensure reproducibility.

3.2.2.2 Color analysis

Biopolymeric walls were examined in their color values by a colorimeter in comparison with HPMC and XG. Each sample (1 g) in a plastic bag (color of plastic bag was initially recorded) was placed on the reflectance port of the colorimeter. The color values that are L*, a*, and b* were measured in triplicates and the values of c* (chroma), and ΔE (total color change) were calculated as the following equations reported by Jang & Koh (2023).

$$c^* = \sqrt{a^{*2}+b^{*2}}$$

$$\Delta E^* = \sqrt{(L_2^*-L_1^*)^2+(a_2^* -a_1^*)^2+ (b_2^* -b_1^*)^2}$$

3.2.2.3 Morphological analysis

Biopolymeric walls were studied with SEM to confirm their morphological details by their microscopic images in comparison with HPMC and XG. Samples were mounted on carbon tape and coated with gold using sputter coater, photographed in a microscope at voltage of 5 keV under the magnification of 200 ×, 500 × and 2000 × followed by measuring pore size with ImageJ software (Yu et al., 2021).

3.2.2.4 Fourier-transform infrared spectroscopy

Biopolymeric walls were analyzed with FTIR (ATR technique) in the range 400-4000 cm^{-1} for 32 scans at resolution 4 cm^{-1} to confirm and monitor the interactions between each polymer in a comparison with HPMC and XG (Jaiturong et al., 2020).

3.2.2.5 Differential scanning colorimetry

Biopolymeric walls were investigated for their thermal characteristics by DSC apparatus in triplicate by comparing with HPMC and XG. The sample (3–4 mg) was placed in an aluminum pan and heated in the range of 10–220°C (10°C/min) under a nitrogen purge at the rate of 50 mL/min (Pueknang & Saewan, 2022). An empty aluminum pan was used as a reference. The temperature of onset (T_o), melting peak (T_m), and endset (T_e) were computed automatically from the thermograms.

3.2.2.6 X-Ray diffraction analysis

Biopolymeric walls were further assessed with X-ray diffraction analysis in triplicate by comparing with pure HPMC and XG. The samples were analyzed at 40 kV and 30 mA with CuKα radiation, at a scanning rate of 1.0°/min over the 2θ range of 5° to 30° (Pueknang & Saewan, 2022). The values of 2 theta (2θ) were calculated using X'Pert HighScore Plus program.

3.2.3 Physicochemical properties of biopolymeric walls

Physicochemical properties of biopolymeric walls (water solubility index, water absorption rate, and swelling capacity) were determined, following a slightly modified method from Navarro-Flores et al. (2020). Sample (25 mg) was added to 10 mL of deionized water and mixed for uniform dispersion. The mixture was incubated at 30°C for 30 minutes and centrifuged at 3500 rpm at 25°C for 10 minutes. The supernatant was collected in a petri dish and dried in hot air oven at 105°C to a constant weight. The experiment was done in triplicate. WSI, WAR, and SC were calculated as follows.

$$\text{WSI} = \frac{\text{Supernatant dried weight}}{\text{Initial weight microcapsules}} \times 100$$

$$\text{WAR} = \frac{\text{Fresh sediment weight}}{\text{Initial weight microcapsules}}$$

$$\text{SC} = \frac{\text{Supernatant dried weight}}{\text{Initial weight microcapsules} \times (100\text{-WSI})}$$

3.2.4 Preparation of encapsulated FA in biopolymeric walls

Biopolymeric walls were loaded with FA following a modified method from the study of Yu et al. (2021). Initially, HPMC gradually dispersed in RO water under water bath heating (70 °C) to ensure complete dissolution, followed by an addition of XG (except FABW4) under a continuous mixing. The mixture was then homogenized at 10,000 rpm and subsequently hydrated at 4 °C for 24 h. Aftermath, FA solution 11% w/w (in ethanol) was incorporated at 1.22–1.23% (w/w) into the polymer solution using two different steps: (i) before hydration (BF), where FA was added directly into the freshly prepared polymer mixture prior to hydration, and (ii) after hydration (AF), where FA solution was added into the pre-hydrated polymer mixture. Following FA addition, all formulations were subjected to pre-freezing at −40 °C and freeze-dried under vacuum (<1 mbar) for 24 h.

Table 3.4 Composition of encapsulated FA in biopolymeric walls

Formula	FA	Ethanol	HPMC	XG	Water	Total weight	% of FA
$FABW1_{BF}$	1	8.1	2.5	0.05	70	81.65	1.22
$FABW1_{AF}$	1	8.1	2.5	0.05	70	81.65	1.22
$FABW2_{BF}$	1	8.1	2.5	0.02	70	81.62	1.23
$FABW2_{AF}$	1	8.1	2.5	0.02	70	81.62	1.23
$FABW3_{BF}$	1	8.1	2.5	0.01	70	81.61	1.23
$FABW3_{AF}$	1	8.1	2.5	0.01	70	81.61	1.23
$FABW4_{BF}$	1	8.1	2.5	-	70	81.60	1.23
$FABW4_{AF}$	1	8.1	2.5	-	70	81.60	1.23

Note Subscript BF= FA added before hydration, AF= FA added after hydration

3.2.5 Characterization and properties of encapsulated FA

Characterization assays (color analysis, SEM, FTIR, DSC, XRD) and physicochemical properties (water solubility index, water absorption rate, swelling capacity) of encapsulated FA and free FA were assessed under the same methods as performed for biopolymeric walls.

3.2.6 Encapsulation efficiency

The experiment of encapsulation efficiency was adapted from the study of Yu et al. (2021). First, FA quantification was conducted using UV–Vis spectrophotometry. A stock solution (1000 ppm) was prepared by dissolving FA in methanol, followed by serial dilutions (0.5–8 ppm) to create a FA calibration curve at the maximum absorption wavelength (λ_{max}). Methanol was used as blank, and all measurements were performed in triplicate.

About 20 mg of the encapsulated FA was dissolved in 10 mL of methanol for 72 h at room temperature. The mixture was sonicated for 10 minutes at 25 °C then centrifuge at 9000 rpm for 10 minutes. The supernatant (free FA) was collected, and its absorbance was recorded using UV-Vis spectrophotometry at λ_{max}, with the FA calibration curve. All the tests were done in triplicate, and encapsulation efficiency (EE) expressed as a percentage was calculated according to the following equation.

$$\text{EE (\%)} = \frac{\text{Weight of initial FA loaded - weight of free FA}}{\text{Weight of initial FA loaded}} \times 100$$

3.2.7 Controlled release of encapsulated FA

Controlled release experiment of the encapsulated FA was performed to determine the releasing (percentage) of FA in accordance with the modified method from the study of Pattnaik et al. (2018). The encapsulated FA (10 ppm) was suspended in phosphate-buffered saline (0.15 M, pH 7.4) and the mixture was vortexed to ensure homogeneity and incubated at 37°C under gentle agitation using an incubator shaker. At different time intervals (1, 1.5, 2, 2.5, 3, 4, 6, 24, 48, and 72 h), the aliquots (1 mL) were withdrawn, then replaced with the same volume of PBS, centrifuged at 8000 rpm for 10 minutes to separate the released FA, and the supernatant was used in UV-Vis spectrophotometry to measure its absorbance at 324 nm. All measurements were performed in triplicate. The percentage of cumulative FA releasing was computed from the following equation.

$$\text{Release (\%)} = \frac{\text{Amount of FA released at time t}}{\text{Total FA loaded in biopolymer walls}} \times 100$$

3.2.8 Stability testing of encapsulated FA

Thermal stability test of encapsulated FA and free FA was studied for the duration of 6 months in accordance with ICH guideline similarly with the same method of Banerjee et al. (2014). Samples were put in small glass bottles and kept in the temperature and humidity chamber at 40 ± 2°C and relative humidity (RH) 75 ± 5%. The samples were withdrawn periodically (0, 2 weeks, 1 month, 2 months, 3 months and 6 months) and evaluated their color changes, and encapsulation efficiency. For photostability, the samples were exposed under UVA light adjusting the distance between the bottom of the vial and the light. Photostability was conducted in last week of 6 months period and same parameters were measured.

3.2.9 Statistical Analysis

All experiments were conducted in triplicates and data were shown as mean ± SD for each experiment. Statistical analyses were conducted using SPSS software (SPSS 20.0, IBM, Chicago, IL). One-way analysis of variance (ANOVA) followed by Tukey tests were executed at 95% confidence level to assess significant differences.

CHAPTER 4

RESULTS AND DISCUSSION

4.1 Preparation of Biopolymeric Walls

Four biopolymeric walls (79.74 -73.60 % yield) were prepared and assessed by visual observation. Biopolymeric walls were denoted as BW and despite varying XG amounts, BW appeared as very white, lightweight, and the freeze-dried BW1–BW4 exhibited near-neutral pH values (7.35–7.82) at 10% concentration. HPMC is near neutral (pH 6.35 at 10%), while XG is slightly acidic (pH 5.30 at 10%). A combination of these biopolymers was clearly yielded the neutral vehicle that would be optimized with variety of cosmetic formulations.

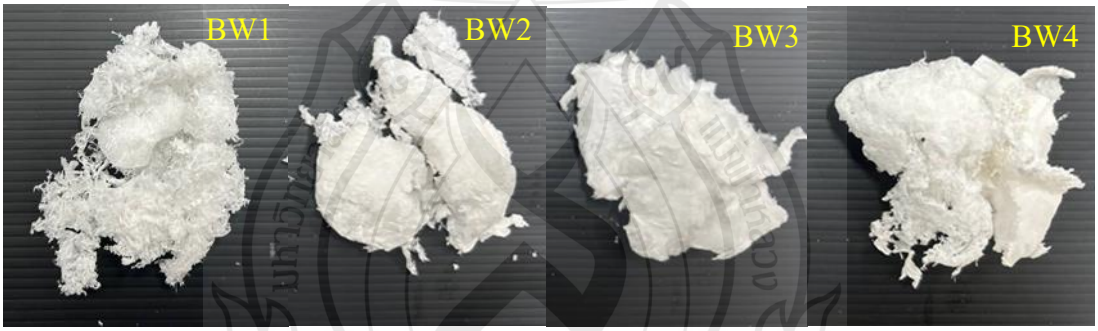

Figure 4.1 The appearance of the fabricated biopolymeric walls

4.2 Characterization of the Biopolymeric Walls

4.2.1 Colorimetric analysis

The color analysis as presented in Table 4.1 showed that all biopolymeric walls were moderate in lightness (L* 44 to 46) suggesting their white to off-white appearance after freeze-drying. BW1, the highest XG, was lowest in L* (44.26 ± 0.87), indicating a slightly darker color due to the color of XG, whereas BW4 without XG exhibited the highest lightness (46.25±0.69), confirming the presence of XG slightly reduced the brightness tone. The a* were close to zero (0.08-0.16), and the redness or greenness can

be negligible. However, b* reduced from BW1 (6.43 ± 0.26) to BW4 (5.24 ± 0.29), affirming that the presence of XG increased yellowness of the walls. Similarly, chroma (c*) shifted from positive to slightly negative as XG content reduced, reflecting declined color saturation. Although BW4 is composed entirely with HPMC, its hydration and freeze-drying leads to differences from HPMC whereas BW4 exhibited slightly lower lightness (L*) than HPMC, which may be associated with changes in surface characteristics after freeze-drying that was observed by SEM analysis showing a transition from the fibrous surface of HPMC to porous network in BW4.

Table 4.1 Colorimetric analysis of the biopolymeric walls, HPMC and XG

Sample	**L***	**a***	**b***	**c***
BW1	44.26 ± 0.87^{b}	0.10 ± 0.06^{b}	6.43 ± 0.26^{c}	0.43 ± 0.26^{b}
BW2	$45.97 \pm 1.58^{b,c}$	0.08 ± 0.08^{b}	$5.89 \pm 0.56^{b,c}$	-0.11 ± 0.55^{b}
BW3	$46.12 \pm 0.35^{b,c}$	0.14 ± 0.03^{b}	$5.34 \pm 0.51^{a,b}$	-0.67 ± 0.51^{a}
BW4	$46.25 \pm 0.69^{b,c}$	0.16 ± 0.02^{b}	$5.24 \pm 0.29^{a,b}$	-0.76 ± 0.29^{a}
HPMC	47.03 ± 0.01^{c}	0.09 ± 0.01^{a}	4.53 ± 0.01^{a}	0.31 ± 0.02^{b}
XG	38.09 ± 0.03^{a}	2.83 ± 0.01^{c}	17.08 ± 0.02^{d}	12.11 ± 0.01^{c}

Note Values are given as mean ± SD. Values in the same column followed by a different letter (a-d) are significantly different ($p < 0.05$).

4.2.2 Morphological analysis

Morphological characterization of biopolymeric walls, HPMC and XG were studied by SEM in Figure 4.2. HPMC showed fibrous morphology with elongated structures on which wrinkling and folding with dense aggregates that was similar to the study of Wan et al. (2021). In contrast, BW4 processed via freeze-drying exhibited a porous, thin-wall structure with a pore size of 37.16 ± 0.86 μm. XG presented granular structure with visible flakes on rough surfaces. The biopolymeric walls demonstrated interconnected, thin walls with pores, being distinct from the morphological patterns of HPMC and XG. As observed by SEM images (500× magnification), XG improves the porosity of the walls which were measured by ImageJ and illustrated in Table 4.2.

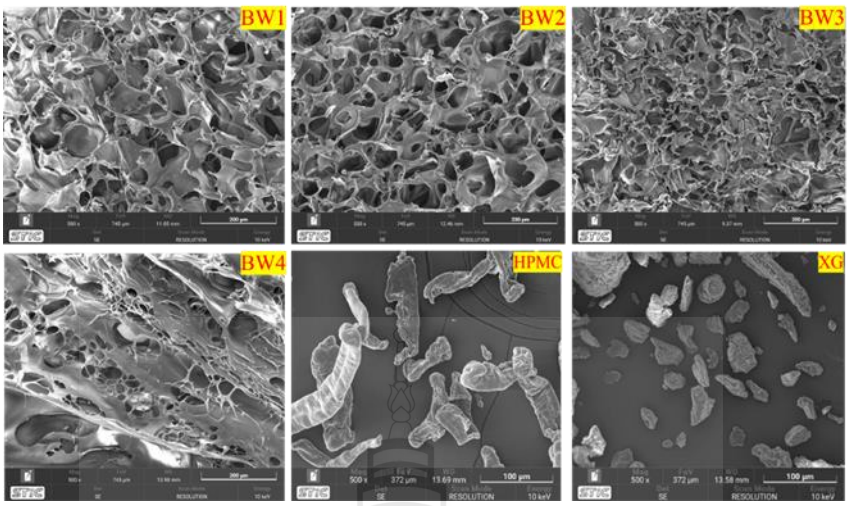

Figure 4.2 Morphology of the biopolymeric walls, HPMC, and XG

4.2.3 FTIR analysis

FTIR spectra of HPMC, XG and the biopolymeric walls are shown in Figure 4.3. HPMC showed a distinct broad spectrum at 3430 cm^{-1} corresponding to O-H stretching while C-H stretching was noted in 2800-3000 cm^{-1}. The band at 1052 cm^{-1} was assigned to C-O stretching and 1453 cm^{-1} refer to C-H bending. The peaks at 1469, 1377, 1317, and 943 cm^{-1} are assigned to the asymmetrical, symmetrical, in-plane and out-plane vibration of $–CH_3$, (Zheng et al., 2022). XG showed O-H stretching at 3279 cm^{-1} due to axial deformation of O-H. Another band at 2914 cm^{-1} related to C-H stretching and 1602 cm^{-1} related with axial deformation of C-O (Naeem et al., 2023).

In the spectrum of the biopolymeric walls, a broad band with reduced intensity and peak position shifted to 3416 cm^{-1} attributed to O-H stretching vibration between -OH of HPMC and -COOH of XG. The presence of HPMC can be confirmed by the C−H stretching band at 2918 cm^{-1}, typical of alkyl groups (CH_2 and CH_3). XG with the asymmetric COO^- showed at 1645 cm^{-1}, confirming XG presence. Additional peaks at 1454 and 1375 cm^{-1} showed characteristic CH_2/CH_3 bendings and XG's carboxylate groups. Finally, a strong peak at 1051 cm^{-1}, correspond to C-O-C and C-O stretching vibrations of the glycosidic linkages and the polysaccharide backbone, showing the biopolymeric wall structure.

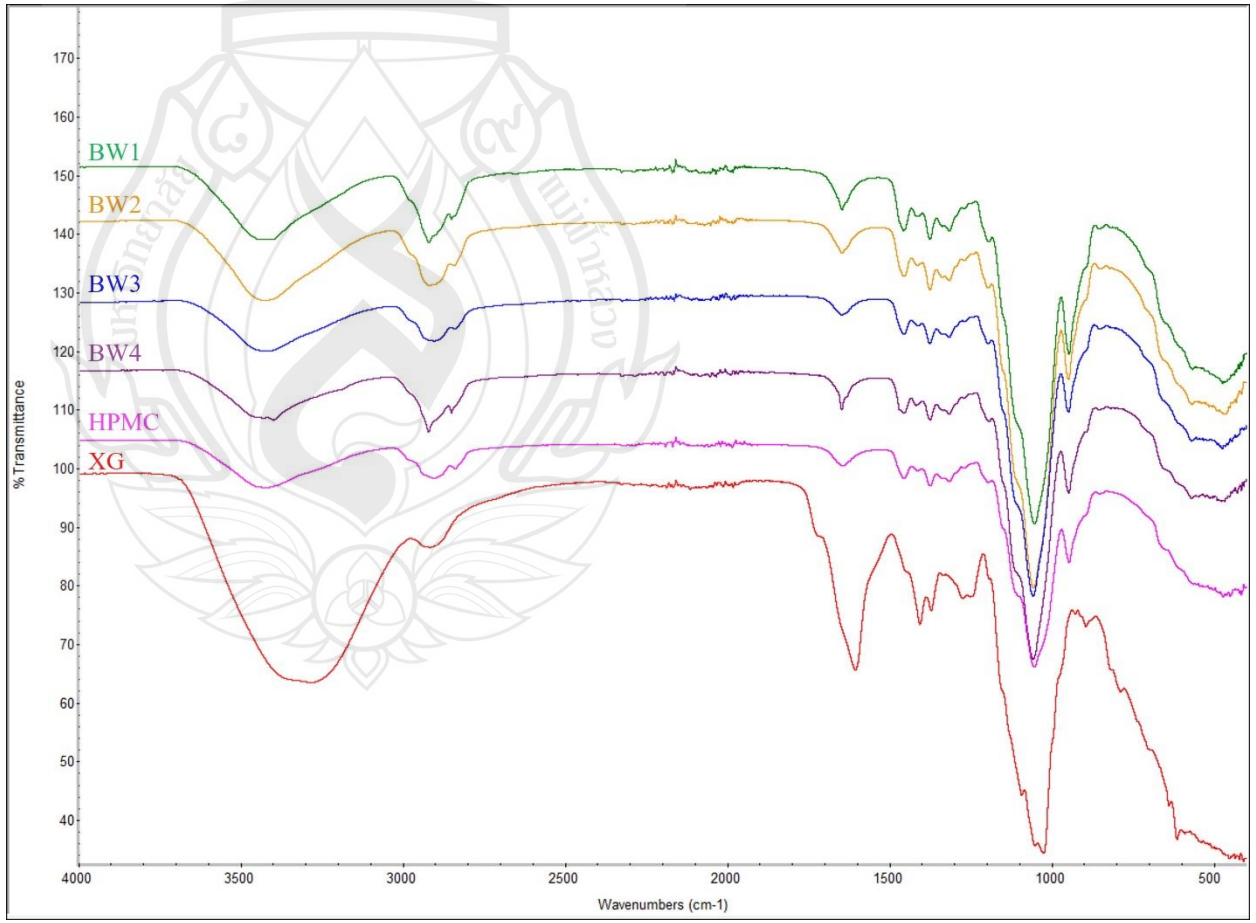

Figure 4.3 FTIR spectra of the biopolymeric walls, HPMC, and XG

4.2.4 Thermal analysis

Thermal characteristics of the biopolymeric walls were studied using DSC and the DSC thermograms of biopolymeric walls, HPMC and XG are shown in Figure 4.4. Pure HPMC exhibited a low intensity broad peak between 40-112°C due to evaporation of loosely bound water in HPMC. XG indicated a stronger, and broader endothermic peak in 49-134°C, whereas melting temperature of XG at 92.67 ± 0.78°C was higher than those of the biopolymeric walls (82.28-83.39°C). However, thermograms of the walls are similar to HPMC, showing its influence with melting temperature of 84.89 ± 4.00°C. The biopolymeric walls (BW1–BW4) exhibited intermediate endothermic peaks, implying successful blending between two polymers. Notably, the peak intensity and position varied slightly with XG content, suggesting that increasing XG changed the thermal behavior of the walls. The absence of sharp melting peaks in all the walls confirmed their amorphous nature, and the shift of endothermic transitions support hydrogen-bond interactions between HPMC and XG. In Table 4.2, the enthalpy of the walls (-122.96 to -139.85 J/g) were lower than HPMC (-161.04 J/g) and XG (-340.95 J/g). This confirms that compatible mixing of HPMC and XG resulted in less crystalline and more amorphous structure. BW4 displayed a broader endothermic transition with reduced enthalpy change compared to HPMC, this indicates a disruption of the semi-crystalline polymer chains and the formation of a more amorphous, disordered structure thus BW4 is considered potential for FA loading.

Table 4.2 Key parameters of the biopolymeric walls, HPMC and XG

Sample	**Pore size (µm)**	**T_m (°C)**	**Enthalpy (J/g)**
BW1	51.49 ± 2.85^{a}	82.95 ± 4.02^{a}	-139.85 ± 8.28^{a}
BW2	44.05 ± 1.35^{b}	82.72 ± 2.04^{a}	-132.72 ± 8.96^{a}
BW3	$41.71 \pm 2.13^{b,c}$	82.28 ± 1.45^{a}	-132.01 ± 8.73^{a}
BW4	37.16 ± 0.86^{c}	83.39 ± 1.62^{a}	-122.96 ± 6.96^{a}
HPMC	n.d.	84.89 ± 4.00^{a}	-161.04 ± 7.22^{b}
XG	n.d.	92.67 ± 0.78^{b}	-340.95 ± 4.82^{c}

Note n.d.= not detected, T_m = melting temperature. Values are given as mean ± SD and values in the same column followed by a different letter (a-c) are significantly different ($p < 0.05$).

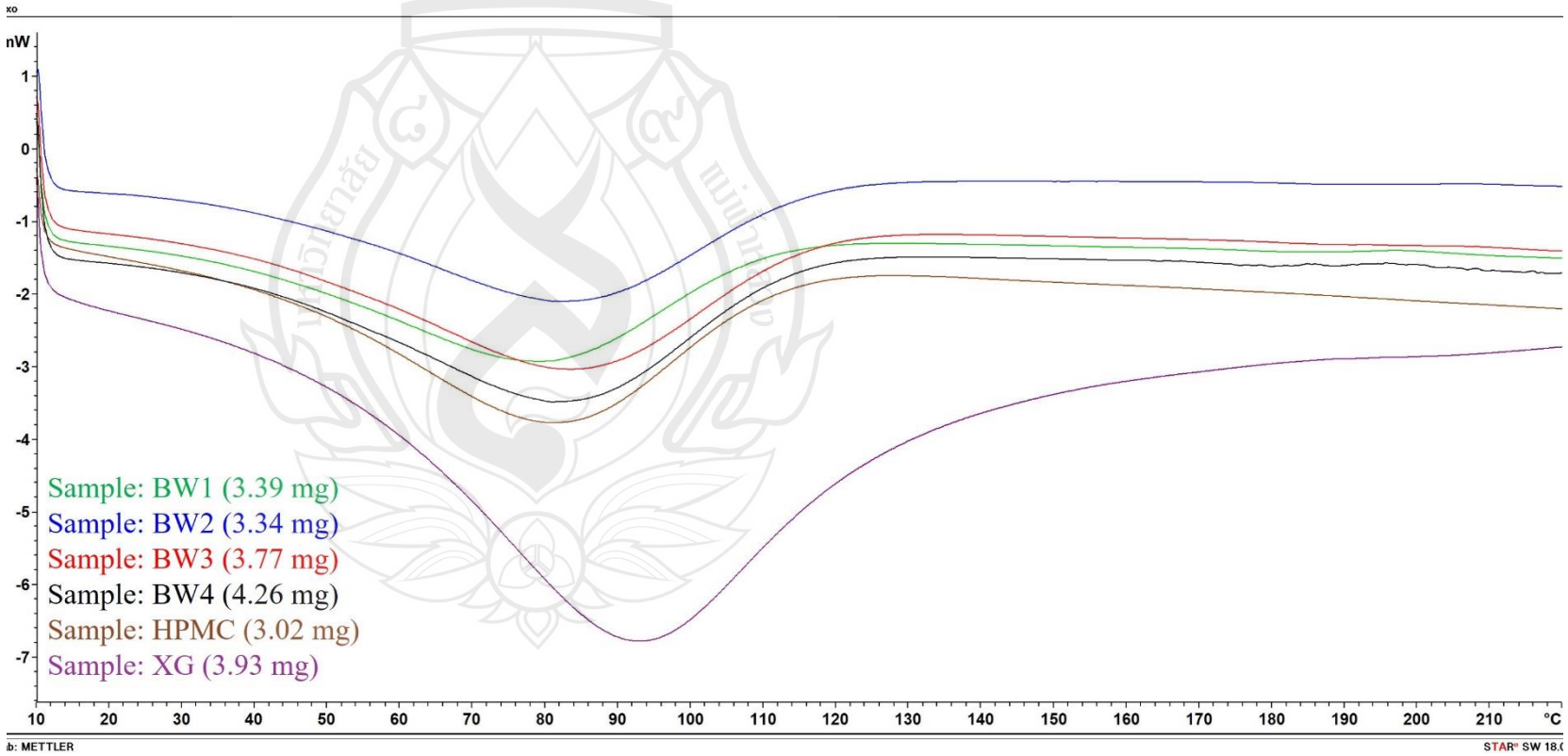

Figure 4.4 DSC thermograms of the biopolymeric walls, HPMC, and XG

4.2.5 X-Ray diffraction analysis

XRD patterns of the biopolymeric walls exhibited broad amorphous halos with reduced diffraction intensities compared to pure HPMC and XG shown in Figure 4.5. HPMC displayed two amorphous peaks at 2θ approximately of 8° and 20°, whereas XG indicated two broad peaks at 2θ of 8 and 19.26, confirming its amorphous nature. The biopolymeric walls (BW1 to BW4) illustrated a progress reduction in the intensity and sharpness of HPMC's diffraction peaks with broader profile at 2θ of 11° and 21°. BW4 exhibited a broader amorphous halo with reduced diffraction intensities compared to HPMC. This transformation indicates that the hydration and freeze-drying disrupted semi-crystalline regions of HPMC, leading to amorphous state the polymer chains in BW4 become more open and flexible, essential for the molecular dispersion of FA. XRD patterns of the biopolymeric walls suggested that disruption of HPMC's ordered regions and the formation of new amorphous structure, resulting from hydrogen bonding between HPMC and XG. Such changes in diffraction pattern align with DSC thermograms, where the endothermic transition of HPMC shifted and less distinct with XG addition. Thereafter, these XRD findings confirm that XG addition induces molecular interaction with HPMC, suppressing its semi crystalline order and producing a stable amorphous structure.

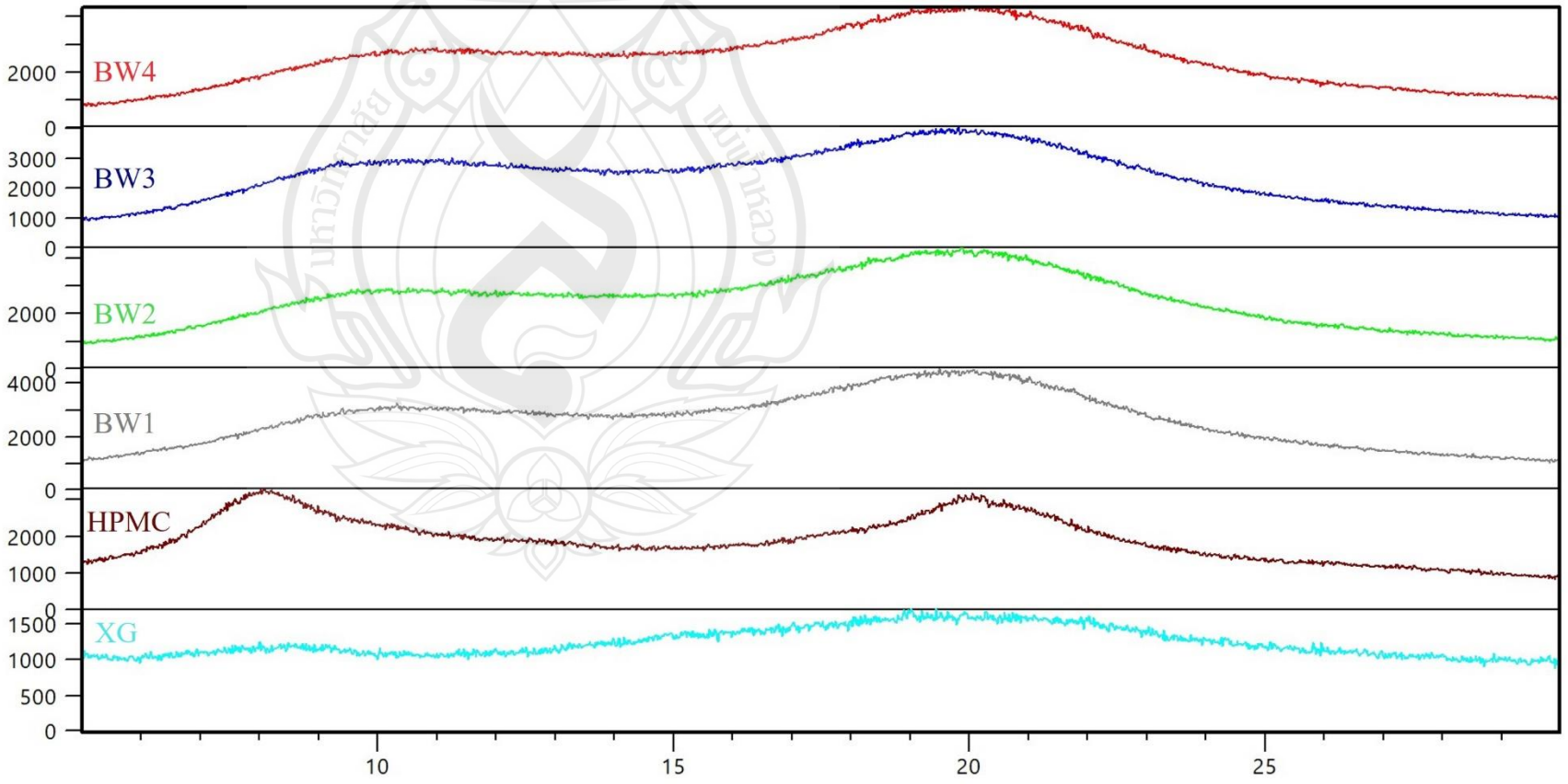

Figure 4.5 The X-ray diffractograms of the biopolymeric walls, HPMC, and XG

4.3 Physicochemical Properties of the Biopolymeric Walls

Physicochemical properties of the biopolymeric walls in terms of water solubility index (WSI), water absorption rate (WAR) and swelling capacity (SC) were determined and compared to HPMC and XG in Table 4.3. For WSI, both HPMC and XG implied higher values, 75.65 ± 4.76 % and 71.94 ± 3.64 % respectively, whereas the biopolymeric walls (BW1 to BW4) showed 38.87 % to 30.57 %. The walls with higher concentrations of XG had higher WSI due to availability of polysaccharide chains present in XG and the reduction in WSI with lower XG is attributed to HPMC's gel forming ability, limiting immediate complete dissolution (Paul et al., 2022). WAR followed a similar trend to WSI but showed lower values which increased with XG content due to its ability to form porous networks via hydrogen bonding by its carboxylate groups (Mughal et al., 2011). Similarly, swelling capacity is consistently low (0.004-0.006), more influenced by HPMC's gel forming (SC: 0.032) compared to XG (SC: 0.026). When compared BW4 and HPMC, BW4 demonstrated lower water solubility, absorption, and swelling capacity relative to HPMC, which can be attributed to the stronger gel-forming behavior and reorganization of HPMC chains during freeze-drying that limit rapid hydration and expansion (Paul et al., 2022).

Table 4.3 Physicochemical properties of the biopolymeric walls, HPMC and XG

Sample	WSI (%)	WAR (gg^{-1})	WAR (gg^{-1})
BW1	38.87 ± 2.55^{a}	18.44 ± 1.60^{a}	0.006 ± 0.00^{a}
BW2	32.70 ± 2.36^{a}	18.05 ± 1.46^{a}	0.005 ± 0.00^{a}
BW3	31.44 ± 2.05^{a}	17.48 ± 0.18^{a}	0.005 ± 0.00^{a}
BW4	30.57 ± 2.40^{a}	16.23 ± 5.36^{a}	0.004 ± 0.00^{a}
HPMC	75.65 ± 4.76^{b}	16.11 ± 2.52^{a}	0.032 ± 0.01^{b}
XG	71.94 ± 3.64^{b}	11.69 ± 0.41^{a}	0.026 ± 0.00^{b}

Note Values are given as mean ± SD and values in the same column followed by a different letter (a-b) are significantly different ($p < 0.05$).

4.4 Preparation of Encapsulated FA

The preparation of FA-loaded the biopolymeric walls (FABW) was carried out for all four formulations using two different FA incorporation steps (before hydration, BF; after hydration, AF), resulting eight formulations. Visually, all formulations produced pale yellow dried solid materials with smooth texture, indicating that the fabrication process was reproducible regardless of FA incorporation order as shown in Figure 4.6. However, the order of FA addition did not affect visual color differences, suggesting that polymer composition was the dominant factor influencing their visual appearance. All FABW formulations (Figure 4.7) showed higher pH values, ranging from 4.5 to 5.6 than free FA, favorable for cosmetic applications.

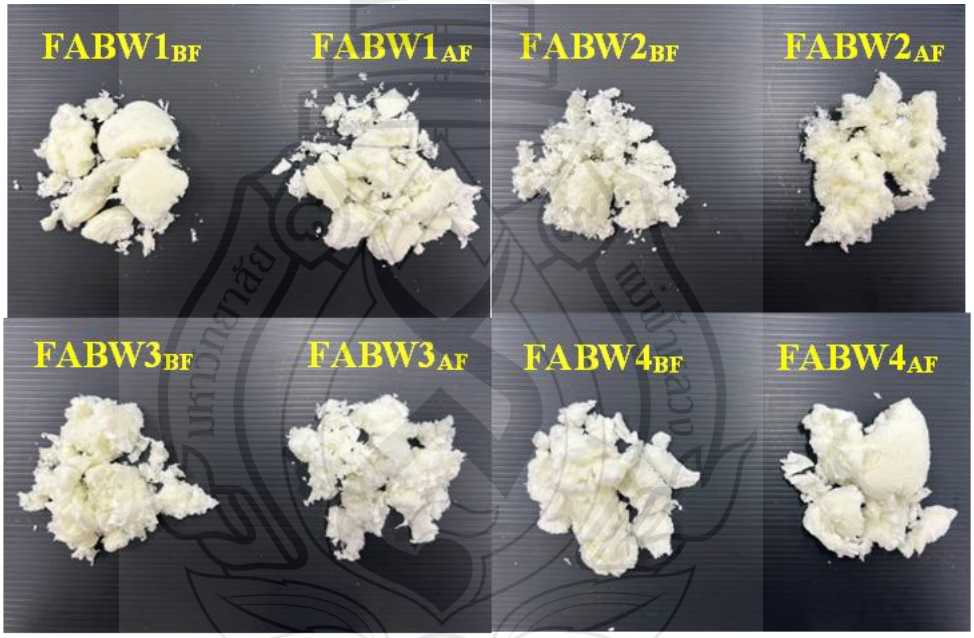

Figure 4.6 Visual appearance of the encapsulated FA

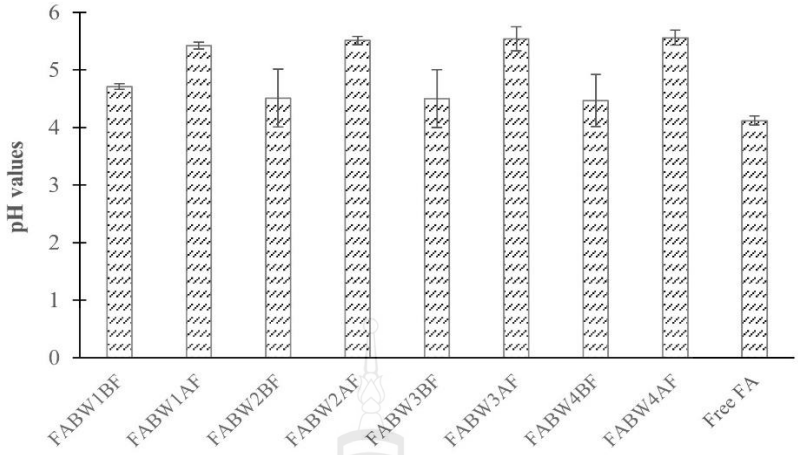

Figure 4.7 pH values of the encapsulated FA and free FA

4.5 Characterization and Properties of the Encapsulated FA

4.5.1 Colorimetric analysis

The color analysis of the encapsulated FA was illustrated in Table 4.4 and FA powder is characterized by a low L* indicating a slightly dark color, a negative a* showing a greenish hue, and a higher b* exhibiting a strong yellowness. The formulations containing higher XG were higher in yellowness (b*) and chroma, while the one with HPMC only showed a slight reduction in yellowness. The higher L* in FABW (41.02 - 43.48) compared to FA (41.28 ± 0.04) showed that encapsulation did not significantly change overall brightness level. All samples, including FA powder, demonstrated negative a*, allowing in the green spectrum, consistent with the original color of FA. The values of b* (15.80 ± 0.07) and c* (15.60 ± 0.06) of FA reduced to b* (9.23- 13.51) and c* (9.12- 13.38) when FA was loaded. A previous study of Torres-Perez et al. (2023) reported colorimetric values of L* (65 ± 2), a* (1.1 ± 0.3), and b* (11.5 ± 0.9) for gluten-free bread containing HPMC 2.04% and XG 1.82%. These values indicated a moderately bright and slightly yellow crumb, which was due to the presence of maize starch, rice flour, and tapioca starch. In contrast, the FA-loaded walls in the present study showed slightly lower L* (41.02–43.48), reflecting the intrinsic color contribution of FA. Nevertheless, encapsulation did not distinctly change the overall brightness compared to FA (L* 41.28 ± 0.04), suggesting that the biopolymeric

walls maintained relatively stable lightness after FA incorporation. The observed range of b* (9.23–13.51) was in line with the previous report b* (11.5) by Torres-Perez et al. (2023), where encapsulation reduced the intense yellowness and chroma of FA (15.80 and 15.60, respectively). This suggested that the walls partially masked yellow color of FA, whereas XG largely contributed to FABW1, possibly due to its pale-yellow color and interaction with FA. The E* of all were close (43.29–44.75), indicating no drastic overall color deviation among the formulations. $FABW_{BF}$ generally results in a slightly less yellow (lower b* and c*), suggesting adding FA before hydration leads to the formulation where the wall materials are more effective at masking the color of FA.

Table 4.4 Colorimetric analysis of the encapsulated FA and FA

Sample	L*	a*	b*	c*	E*
$FABW1_{BF}$	$42.29 \pm 0.03^{b,c}$	-3.03 ± 0.01^{g}	11.20 ± 0.01^{e}	10.97 ± 0.00^{e}	43.85 ± 0.03^{a}
$FABW1_{AF}$	41.02 ± 0.02^{a}	-3.78 ± 0.02^{b}	13.51 ± 0.01^{g}	13.38 ± 0.01^{g}	$43.35 \pm 0.01^{a,b}$
$FABW2_{BF}$	$42.99 \pm 0.00^{d,e}$	-3.38 ± 0.02^{d}	10.12 ± 0.01^{c}	9.99 ± 0.01^{c}	$44.29 \pm 0.00^{b,c}$
$FABW2_{AF}$	$42.43 \pm 0.00^{c,d}$	-3.52 ± 0.02^{c}	12.94 ± 0.01^{f}	12.77 ± 0.01^{f}	$44.50 \pm 0.00^{d,e}$
$FABW3_{BF}$	43.48 ± 0.01^{f}	-3.98 ± 0.02^{a}	9.78 ± 0.01^{b}	9.83 ± 0.01^{b}	44.75 ± 0.00^{e}
$FABW3_{AF}$	$42.20 \pm 0.58^{b,c}$	-3.22 ± 0.02^{e}	11.25 ± 0.02^{e}	11.05 ± 0.02^{e}	$43.79 \pm 0.56^{a,b}$
$FABW4_{BF}$	$42.61 \pm 0.04^{c,d}$	-3.34 ± 0.07^{d}	9.23 ± 0.09^{a}	9.12 ± 0.08^{a}	$43.73 \pm 0.02^{a,b}$
$FABW4_{AF}$	41.76 ± 0.05^{b}	-3.18 ± 0.02^{f}	10.98 ± 0.05^{d}	10.78 ± 0.05^{d}	43.29 ± 0.04^{a}
FA	41.28 ± 0.04^{a}	-3.66 ± 0.03^{b}	15.80 ± 0.07^{h}	15.60 ± 0.06^{h}	$44.35 \pm 0.06^{c,d}$

Note Values are given as mean ± SD and values in the same column followed by a different letter (a-h) are significantly different ($p < 0.05$).

4.5.2 Morphological analysis

The morphological characterization of the encapsulated FA was studied using SEM (Figure 4.8). FA appeared as needles like crystals, and some are spherical and semi spherical to rosette like amorphous aggregates. That will be notified once FA was loaded (Yu et al., 2021). However, porosity could not be detected for all encapsulated FA, which is likely due to the distribution of FA particles. The particles then occupy the pores and surface cavities of the walls when observed by SEM. Morphological analysis confirmed the transition of FA crystals into more dense, amorphous forms. This suggested that FA-loaded walls were districted from each polymer, which can be

clearly seen that the inclusion of particles showed FA irregular pieces of amorphous aggregates and the FA original morphology was changed.

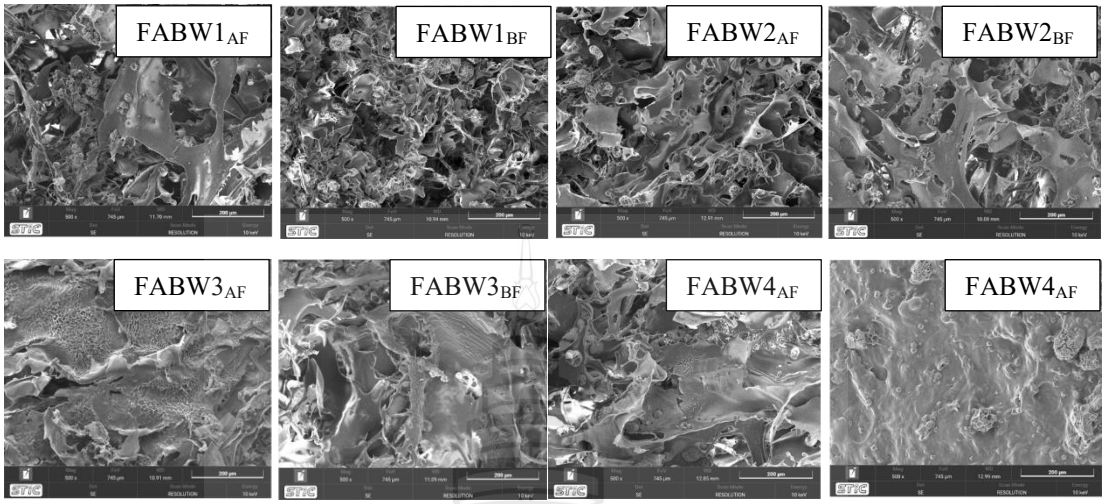

Figure 4.8 Morphology of the encapsulated FA under 500 × magnification

4.5.3 FTIR analysis

FTIR confirmed successful encapsulation of FA (Figure 4.9 to 4.12). Free FA showed O–H (3432 cm^{-1}), C=O (1688 cm^{-1}), C=C (1618-1431 cm^{-1}), C–O–C (1266 cm^{-1}) and out of plane C–H peaks at 851–803 cm^{-1} indicating the presence of two hydrogen atoms next to phenyl ring of FA (Wang et al., 2011). FA encapsulation was confirmed through: (1) O–H broadening at 3420 cm^{-1}, (2) retention of biopolymeric walls (C–H at 2918 cm^{-1} and C–O C at 1051 cm^{-1}), (3) shifted peaks of COO^- at 1619 cm^{-1} where the phenolic hydrogen of FA bonds to the carboxylate oxygen of XG, and (4) disappearance of FA crystalline peaks in 1690 cm^{-1} to 1660 cm^{-1}, where the absence of doublet peaks of FA carbonyl (C=O) conferring changing of FA crystallinity. Similar trends were observed at 1517 cm^{-1} for an aromatic ring vibration and 1277 cm^{-1} for a phenolic C–O stretching.

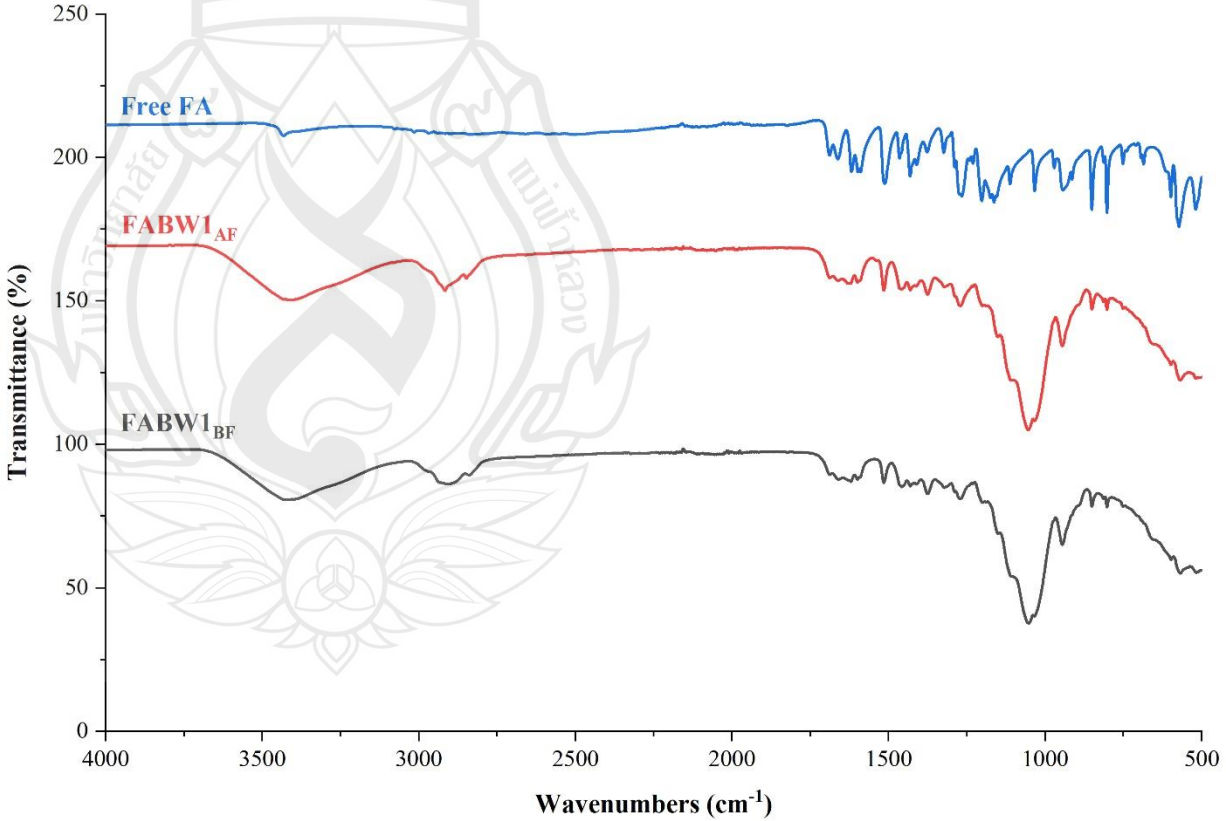

Figure 4.9 FTIR spectra of the encapsulated FA (FABW1) and free FA

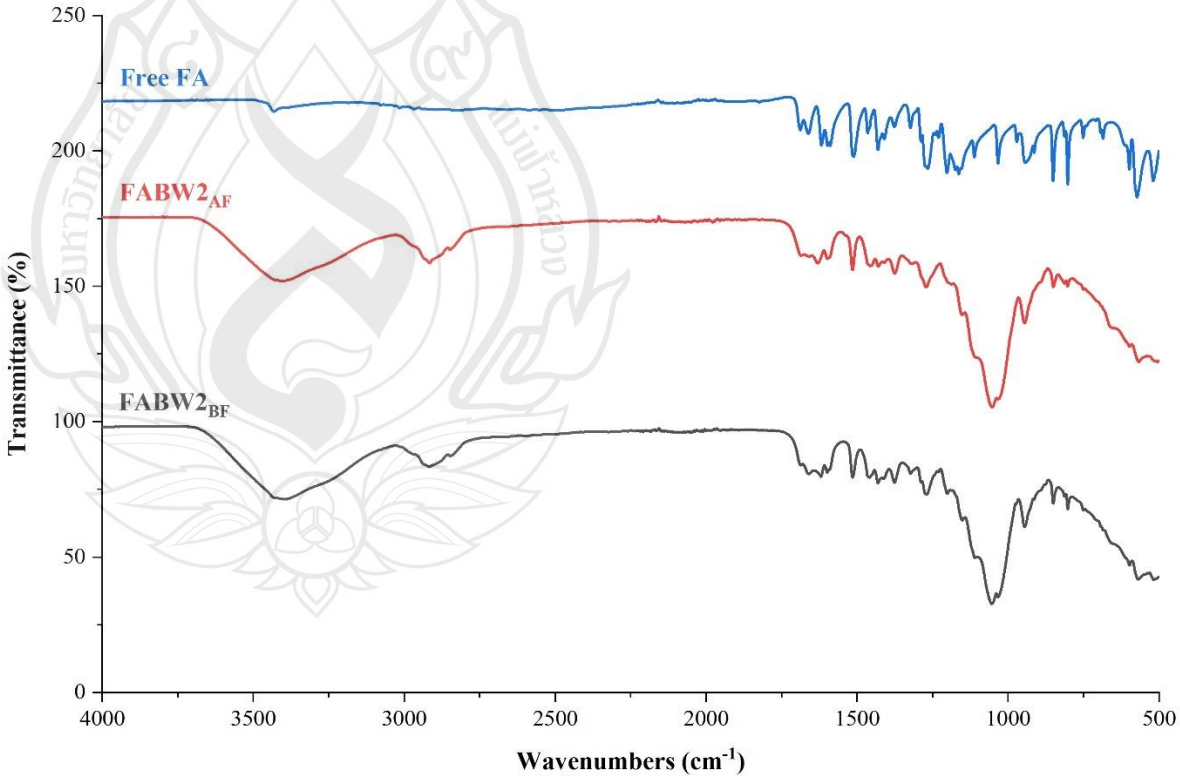

Figure 4.10 FTIR spectra of the encapsulated FA (FABW2) and free FA

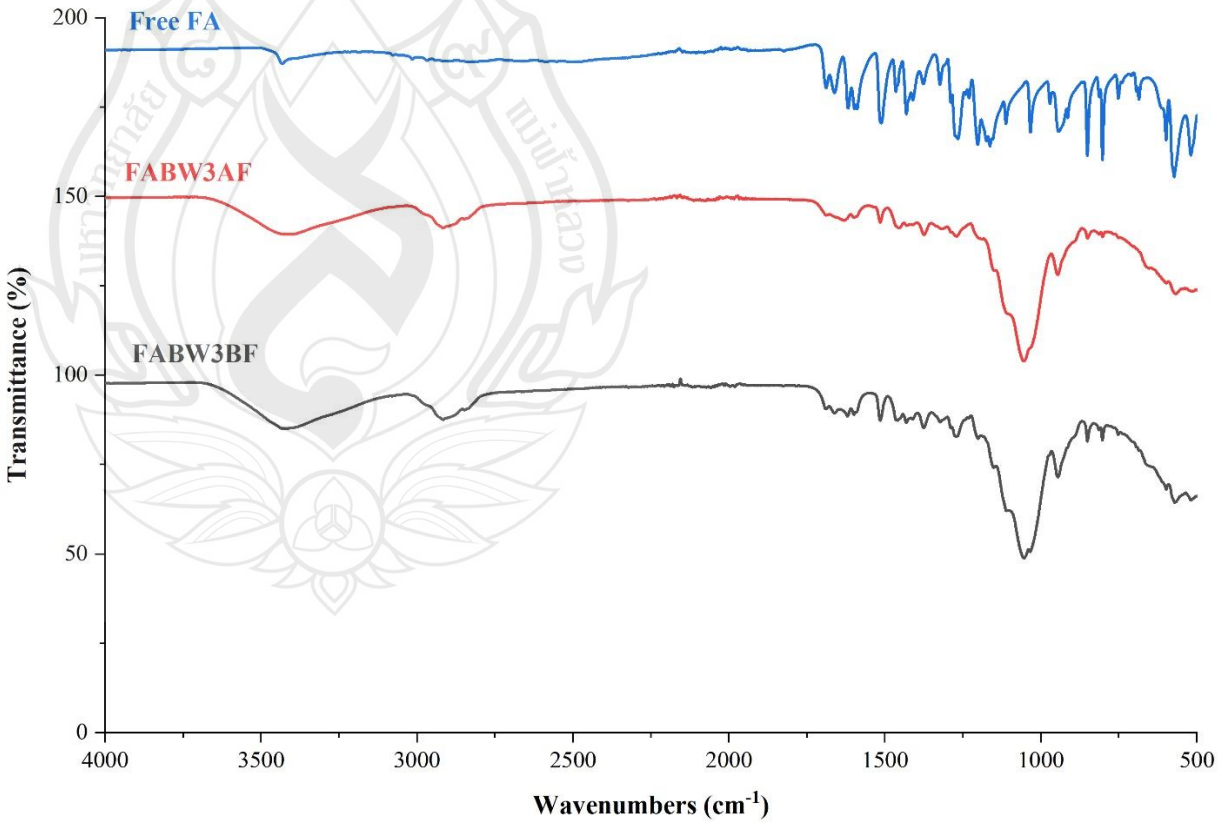

Figure 4.11 FTIR spectra of the encapsulated FA (FABW3) and free FA

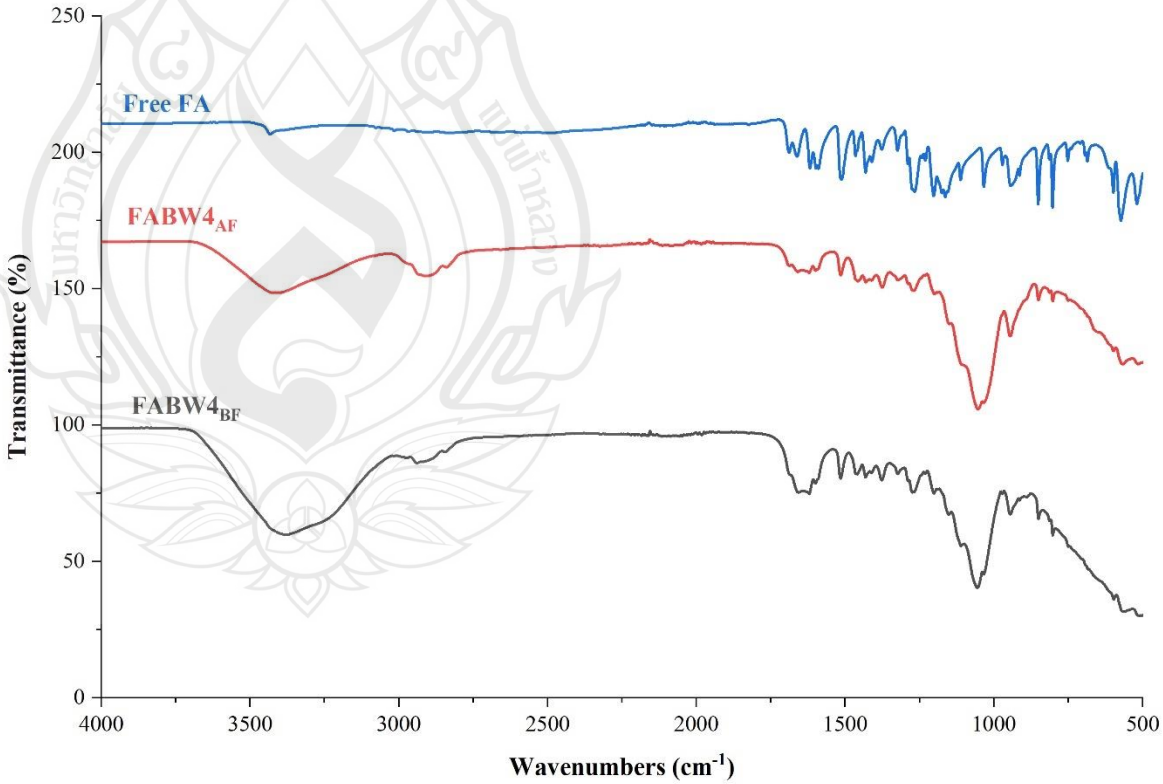

Figure 4.12 FTIR spectra of the encapsulated FA (FABW4) and free FA

4.5.4 Thermal analysis

DSC was used to evaluate thermal characteristics of the encapsulated FA compared to free FA and their DSC curves are shown in Figure 4.13 and 4.14. Free FA showed a single, sharp endothermic peak at 174.86 ± 2.66 °C, which confirms thermal decomposition of its crystalline structure. Free FA started to melt (T_0) at 172.23°C, and its melting process ended at 176.3°C (T_e). A previous study of Sajjadi et al. (2012) reported a sharp endothermic peak of crystalline FA at 168°C (ΔH = 142 J/g). Similarly, from a study of Yu et al. (2023), a sharp endothermic peak of FA was observed at 172°C that in accordance with is close to free FA of this study. In contrast, the thermograms of the encapsulated FA showed a complete disappearance of FA characteristic melting endotherm, however, their thermal characteristics were influenced by broad endothermal transitions. Previously, FA's crystalline thermal peak disappeared when FA was loaded, formation of broad endothermal peaks, implying uniform dispersion of FA (Suksaeree et al., 2014). The absence of FA peaks showed that there was an amorphization by changing from crystalline state to amorphous structure. This observation suggests that DSC thermograms of the encapsulated FA reflect the thermal characteristics of wall materials rather than that of free FA. Significant difference ($p<0.05$) was noted in the range (73.37-79.89°C), with the lowest melting temperature in FABW1 being significantly lower than FABW4, demonstrating XG impacts the thermal stability of FA loaded walls. Overall, these thermal findings suggest improved physical stability and a uniform distribution of FA particles in encapsulation system.

From DSC analysis, BF formulations with more negative ΔH indicate a lower measured enthalpy change (−90.06 to −127.94 J/g) compared to AF formulations (−86.64 to −97.80 J/g), indicating a greater energy absorbed for the transition likely due to disruption of stronger polymer-FA interactions, where more energy required during a transition (Blanco & Siracusa (2021). This larger thermal event indicates higher physical stability in encapsulation systems, as stronger intermolecular forces reduce molecular mobility and leakage under stress (e.g., heat, humidity), enhance physical stability, shelf-life and controlled release (Fonseca et al., 2021).

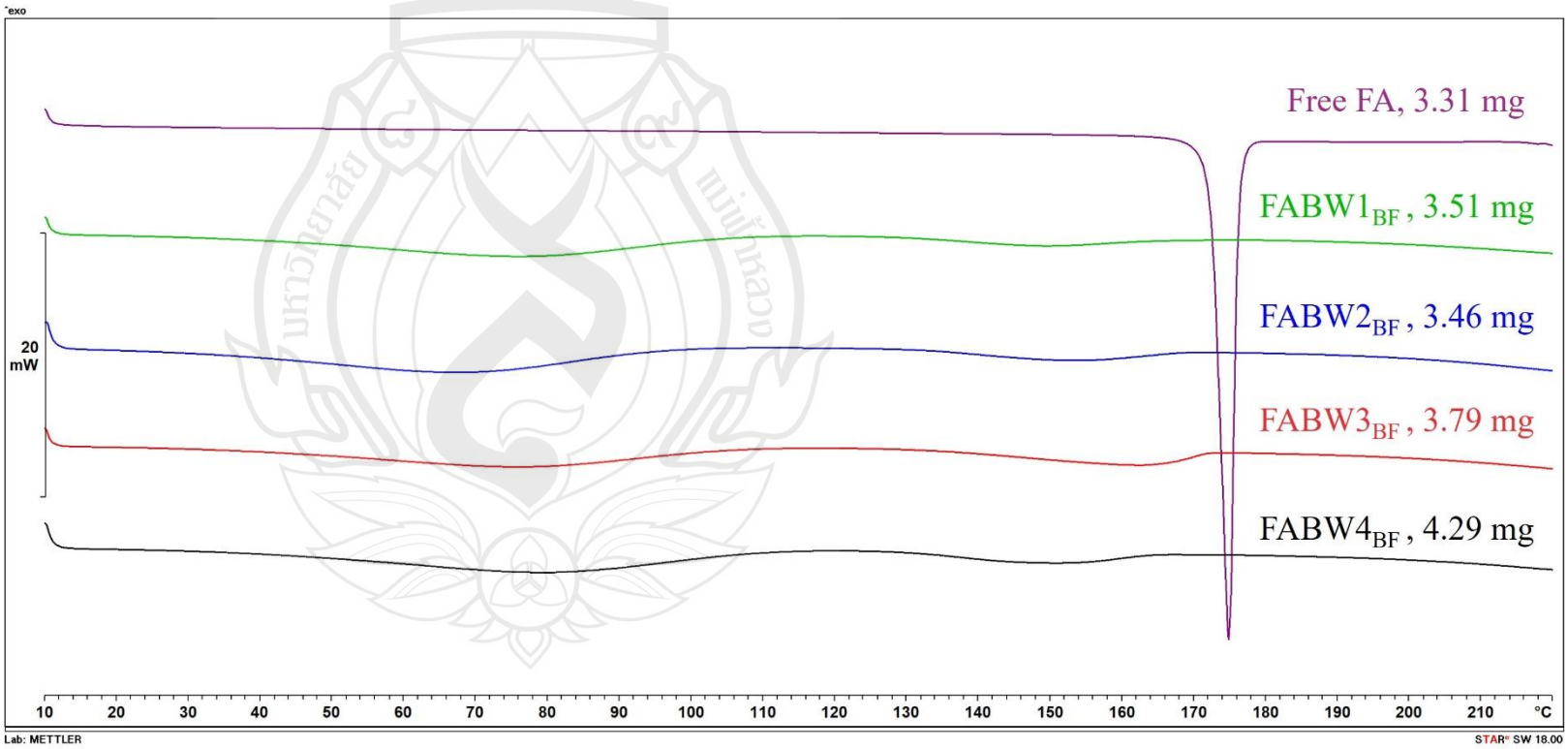

Figure 4.13 DSC thermograms of the encapsulated FA ($FABW_{BF}$) and free FA

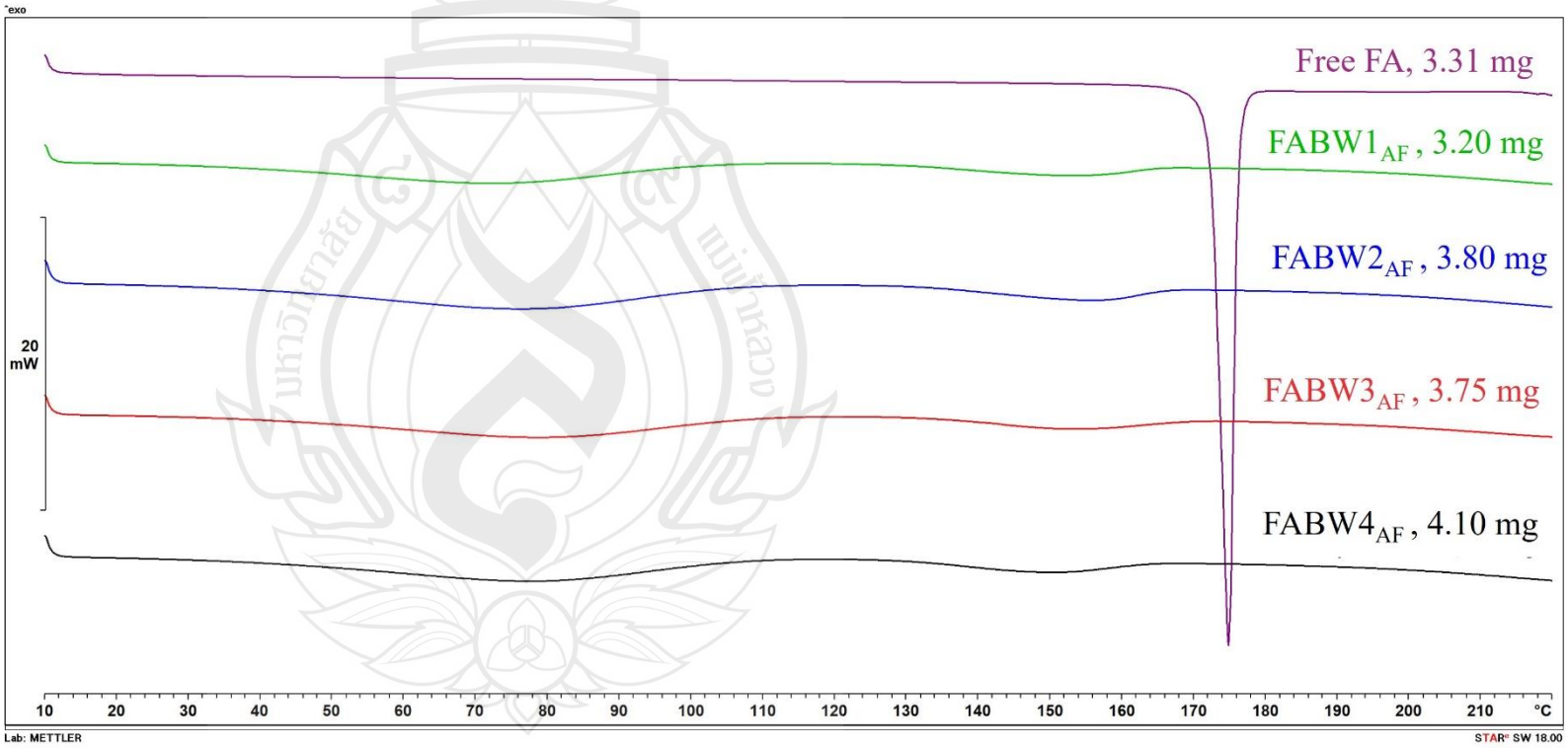

Figure 4.14 DSC thermograms of the encapsulated FA ($FABW_{AF}$) and free FA

Table 4.5 DSC parameters of the encapsulated FA and free FA

Sample	T_0 (°C)	T_m (°C)	T_e (°C)	ΔH (J/g)
$FABW1_{BF}$	37.31 ± 2.47^{a}	$76.91 \pm 2.03^{a,b}$	111.95 ± 7.72^{a}	-127.94 ± 21.26^{b}
$FABW1_{AF}$	36.64 ± 0.84^{a}	73.37 ± 1.09^{a}	111.55 ± 8.75^{a}	$-97.80 \pm 5.14^{b,c}$
$FABW2_{BF}$	35.75 ± 3.40^{a}	81.33 ± 3.06^{b}	108.79 ± 11.60^{a}	-126.28 ± 13.82^{b}
$FABW2_{AF}$	37.15 ± 0.72^{a}	$77.35 \pm 0.93^{a,b}$	111.70 ± 5.12^{a}	$-95.32 \pm 7.38^{b,c}$
$FABW3_{BF}$	38.73 ± 2.05^{a}	79.20 ± 0.58^{b}	107.35 ± 1.86^{a}	-111.37 ± 24.99^{b}
$FABW3_{AF}$	39.11 ± 3.12^{a}	$78.63 \pm 1.91^{a,b}$	106.43 ± 2.68^{a}	$-93.47 \pm 3.41^{b,c,d}$
$FABW4_{BF}$	39.55 ± 1.41^{a}	80.59 ± 0.67^{b}	104.83 ± 3.71^{a}	$-90.06 \pm 6.13^{c,d}$
$FABW4_{AF}$	38.64 ± 0.41^{a}	79.89 ± 2.09^{b}	107.66 ± 1.47^{a}	-86.64 ± 3.16^{d}
Free FA	172.02 ± 1.41^{b}	174.86 ± 2.66^{c}	176.43 ± 1.19^{b}	-164.88 ± 6.76^{a}

Note T_0, onset temperature; T_m, melting temperature; T_e, endset temperature; ΔH, enthalpy change. Values are given as mean ± SD. Values in the same column followed by a different letter (a-d) are significantly different ($p < 0.05$).

4.5.5 X-Ray diffraction analysis

The X-Ray diffractograms of the encapsulated FA and free FA are shown in Figure 4.15 and 4.16. The diffraction patterns of free FA showed its strong crystalline sharp peaks at 2θ of 9.00°, 10.54°, 12.81°, 15.73°, 17.44°, and 26.48° while small peaks occurred at 2θ of 18.18°, 20.49°, 21.21°, 22.43°, 23.10°, 24.57°, 24.80°, 25.98°, 29.04° and 29.43° corresponding to the crystallinity of FA, which conformed with the previous report by Yu et al. (2023) (10.4°, 12.7°, 15.6°, 17.3°, 26.3°, and 29.4°, respectively). In contrast, the XRD patterns of the encapsulated FA are similar to biopolymeric walls, where the suppression of XG's structure and the absence of FA's crystalline peaks was observed, confirming FA was successfully encapsulated in the biopolymer walls. Encapsulated FA exhibited a reduced crystallinity in 20°–30°, re-confirming a successful encapsulation of FA within the walls. Which, its diffraction pattern was clearly distinguished from the individual confirming changes from crystalline to amorphous form (Mahdavi et al., 2016). Accordingly, XRD indicated the encapsulation of FA.

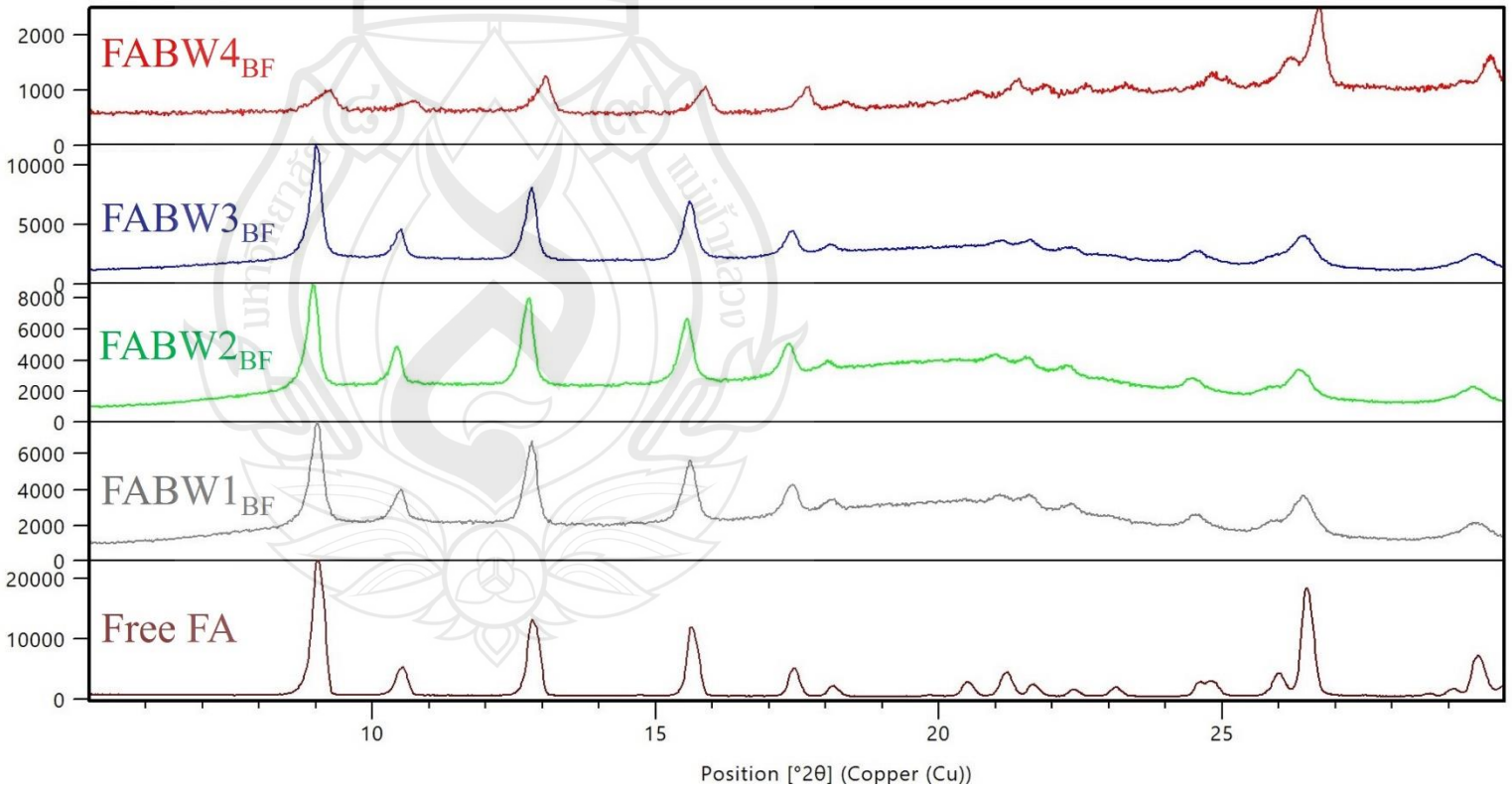

Figure 4.15 X-ray diffractograms of the encapsulated FA ($FABW_{BF}$) and free FA

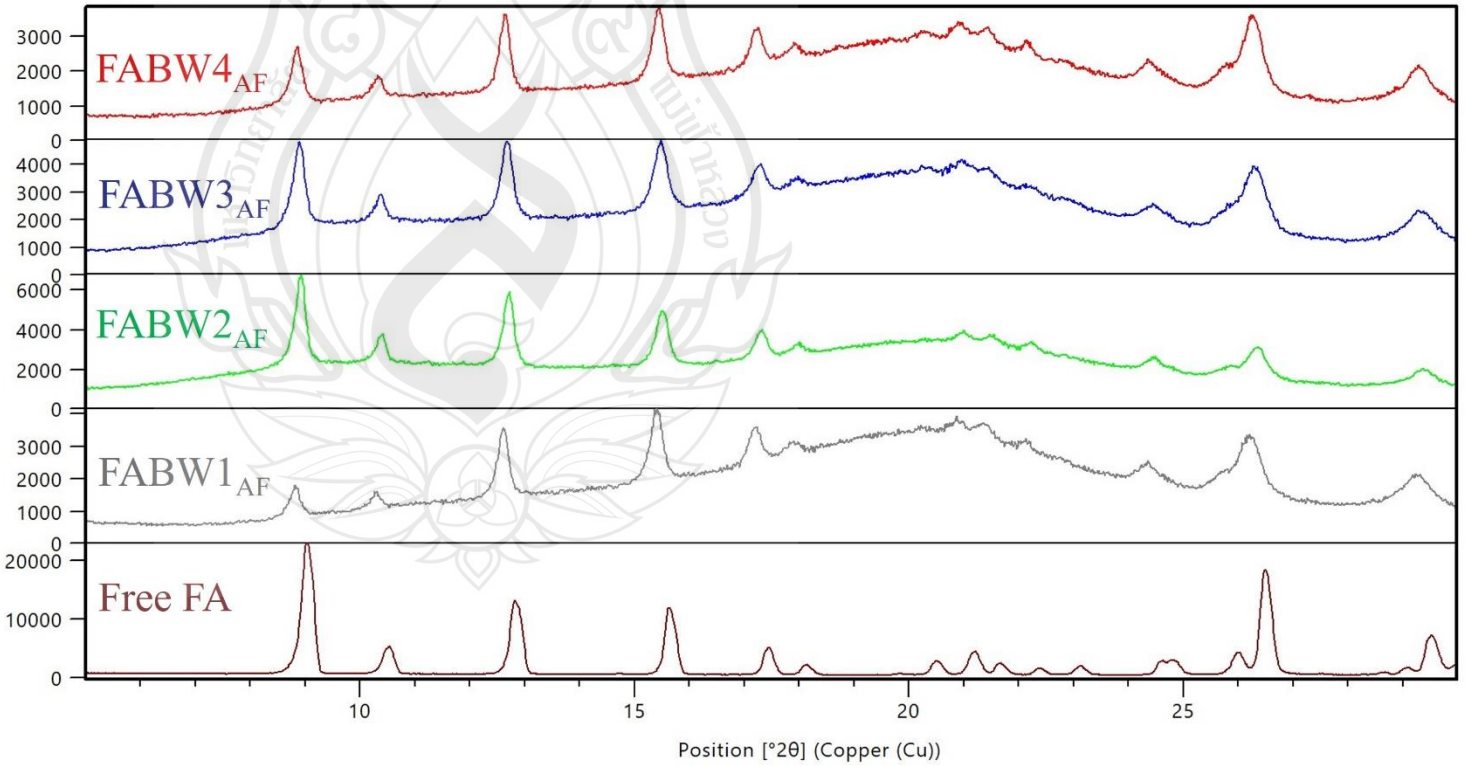

Figure 4.16 X-ray diffractograms of the encapsulated FA ($FABW_{AF}$) and free FA

4.5.6 Physicochemical properties

The physicochemical properties of the encapsulated FA and free FA were summarized in Figure 4.17. The results indicated that XG content and FA addition order significantly affecting the hydration behavior of the encapsulated FA. FABW1 with highest XG exhibited the highest WSI due to the presence of the soluble XG chains and open larger pores observed in SEM images. Meanwhile, AF formulations showed higher WAR but lower WSI, attributed to pre-hydrated polymer networks that allowed greater water uptake. Swelling capacity (SC) followed a similar trend to WAR but remained very low overall, indicating a stable system with controlled hydration properties. Generally, encapsulated FA with lower concentration of encapsulating agent had lower WSI and WAR than that of encapsulated with higher concentration, probably due to the difference in granular structure (Ahmed et al., 2010). The reduced intensity and broadening of characteristic FA peaks in FTIR, together with partial crystallinity in XRD patterns, confirm successful physical entrapment through hydrogen bonding. The morphology further supports the role of XG in forming porous, interconnected structures that enhance water interaction while maintaining encapsulation efficiency.

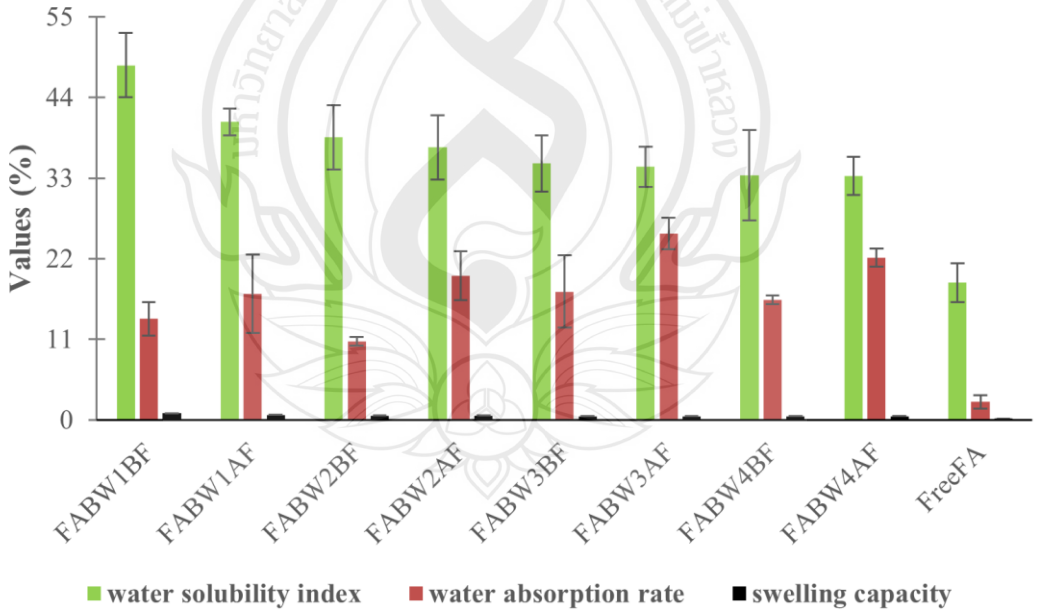

Figure 4.17 Physicochemical properties of the encapsulated FA and free FA

4.6 Encapsulation Efficiency

The encapsulation efficiencies of FABW samples were quantified using UV-Vis spectrophotometry. The standard FA solution showed a maximum absorption wavelength (λ_{max}) at 324 nm when scanned in the range of 200–400 nm using methanol as blank. The wavelength (324 nm) was selected for making the FA calibration curve (shown in appendix A) and subsequent FA quantification. EE results (Figure 4.18) showed a progressive increase in encapsulation efficiency (71.26% to 80.52%) with increasing XG concentrations, indicating that XG plays a critical role in enhancing FA entrapment. FABW4 with HPMC only showed the lowest EE 71.26%, that was lower than all XG-containing formulations ($p < 0.05$). The improved encapsulation noticed in XG-containing walls may be associated with the increased viscosity provided by XG, which could enhance the wall density and promote greater retention of FA within the biopolymeric walls. The results data demonstrated that even minimal XG (0.01–0.02g) significantly improves EE compared to HPMC alone, while the highest XG amount (0.05g) provides maximum encapsulation efficiency, which may be associated with intermolecular interactions between the anionic carboxyl groups ($–COO^-$) of XG and the phenolic hydroxyl groups (–OH) of FA, as observed by the spectral changes in FTIR. Additionally, encapsulation is influenced by physicochemical properties of the actives and encapsulating agents (wall materials), including water solubility, molecular size/weight, and sensitivity (Fara et al., 2019). XG concentration was associated with encapsulation efficiency, suggesting that stronger hydrogen bonding between the anionic XG backbone and phenolic FA molecules promote a stable, highly entrapped system (Gao et al., 2025). Regarding the order of FA addition, BF method allows for immediate dispersion throughout polymer network, and less FA remains on the particle surface, resulting in lower FA detected in the supernatant (unencapsulated part), leading to higher encapsulation efficiency. When FA is added after hydration, the biopolymer network is already settled with limited free volume that might reduce diffusion and entrapment of FA molecules. As a result, a larger fraction of FA remained in the supernatant as free FA, leading to lower EE compared to the BF method. These findings aligned with literature showing polysaccharide-based encapsulation with higher

carboxyl groups achieve superior encapsulation efficiencies for phenolic actives, compared to single-polymers, thereby confirming the effectiveness of the HPMC-XG biopolymeric walls as an optimal delivery carrier for FA. The statistical findings ($p<0.05$) confirm that XG plays a critical component for optimizing encapsulation efficiency in biopolymeric walls for FA encapsulation.

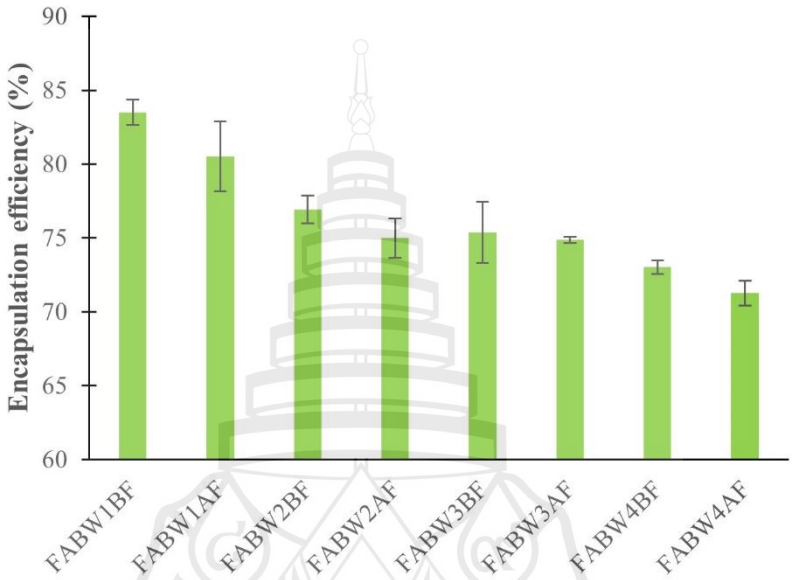

Figure 4.18 Encapsulation efficiencies of the encapsulated FA

4.7 Controlled Release

The controlled release is essential to determine the percentage of release of FA from the encapsulated FA which was plotted against time (h). The quantification of FA release from encapsulated FA was performed through UV-spectrophotometric analysis using FA calibration curve. Figure 4.19 indicated that the release of FA (14.66% - 25.31%) was quite slow for initial 6 h and increased later after 6 h. When compared to FA addition sequence (BF and AF), BF produced more slower, sustained release reaching at maximum 37.97 ± 8.86 % after 72 h, while AF showed 49.07 ± 4.62 % at 72 h, implying faster release. In contrast, BF is likely to allow stronger molecular interactions and deeper entrapment as evidenced by SEM images of BF showing a more uniform structure with fewer surface-exposed crystals, suggesting that the FA particles are embedded, leading to slower and more controlled release. In a study of Pattnaik et

al. (2018), 34% of FA was released in the initial 12 h and reached 67% in 24 h, showing a slower, more sustained release. Conclusively, XG contributes viscosity due to its exceptional swelling and gel formation, allowing pathways for FA release, while FABW4 with HPMC only remained the lowest release, forming less permeable gel, suggesting that XG enhances cumulative release compared to HPMC-only system.

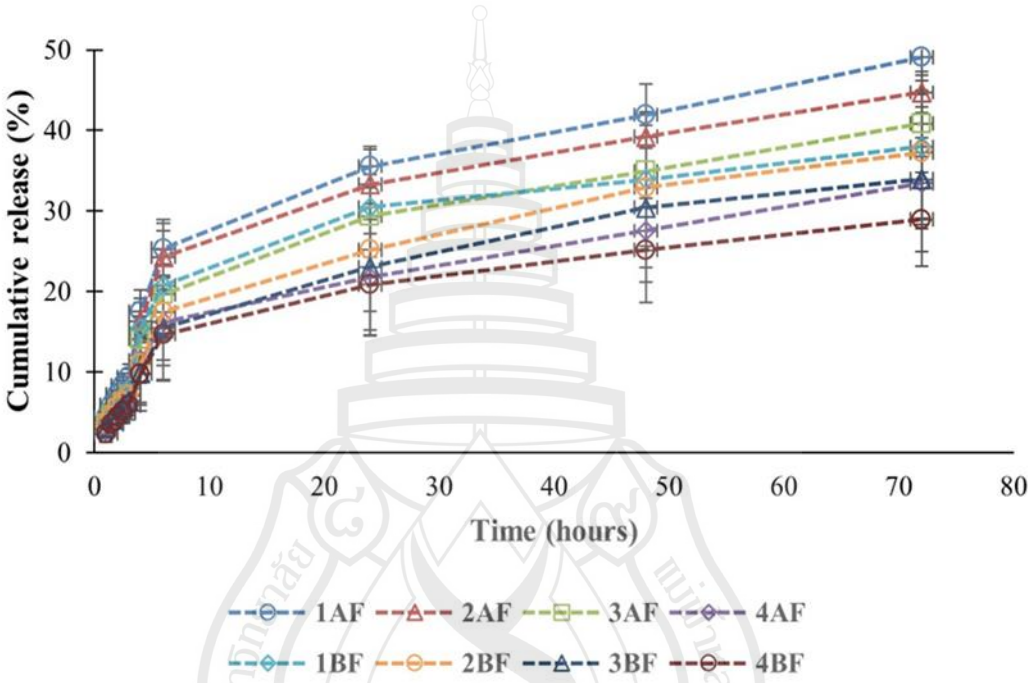

Figure 4.19 Controlled release of FA from the encapsulated FA

4.8 Stability Testing

Stability studies were conducted to assess the effectiveness of FA loaded in the biopolymeric walls over time. FA loaded walls were stored in temperature and humidity chamber under conditions (40 ± 2°C and 75 ± 5% relative humidity) required by ICH guideline. The stability (Figure 4.20) showed a slight reduction in the encapsulation efficiency in the first 2 months but gradually decreased over 6-month storage period. Initially, EE ranged from 71.26-83.49% for all FA loaded walls, even so it declined to 48.82-62.88% after 6 months, indicating a leakage of some FA particles from the biopolymeric walls over time. Notably, BF formulations withstood thermal stress than AF, demonstrating stable EE, and suggesting FA addition before hydration would enable better FA molecular entrapment in the walls, resulting in FA retention over time. For instance, $FABW1_{BF}$ showed initial EE at 83.49% and reached final EE at 62.88%, outperforming $FABW1_{AF}$, which started at 80.52% and fell to 60.55%. Additionally, formulations like FABW1 with higher XG enhanced EE compared to HPMC-only systems (BW4), featuring the XG can optimize molecular interactions that restrict FA mobility. XG-containing nanoparticles have been shown to stabilize polyphenols, improve thermal stability, and keep high retention under accelerating thermal conditions (Rezagholizade-shirvan et al., 2024). Previously, Pueknang & Saewan (2022) reported FA encapsulation in phosphorylated rice starch (EE 73%) improved stability at 45 °C/80% RH, where encapsulated FA retaining ~70% after 30 days. The present study showed FABW1 retained EE of 62.88% even after an extended 6-month period that provides an enduring barrier against active mobilization.

The colorimetric analysis was also monitored under thermal stability testing to assess their color changes over time. L* (Figure 4.21), representing lightness, showed a progressive decline across all formulations over the 6-month storage period, indicating gradual darkening during stability testing. Initially, all FA-loaded walls presented comparable lightness 41–44, which finally dropped to 15.32–29. Among all, FA loaded walls with highest XG revealed better retention of L* compared to those with lower XG content or HPMC-only (FABW4), which was the most decline in lightness. For a*, all FABW samples unchanged, confirming the persistence of this

tone; however, the negative a* slightly declined over time, showing a shift particularly in AF formulations. The b* (yellowness) surged with time in all samples, reflecting progressive yellowing. This pattern was more observed in $FABW_{AF}$ and in general, suggesting relatively better color stabilization in the XG-containing FA loaded walls (Figure 4.22).

Correspondingly, ΔE values decreased over time, stipulating overall darkening. Total color difference (ΔE) increased with time as illustrated in Figure 4.23, exceeding the threshold for visual change, after 3 and 6 months. Notably, FABW1 with higher XG exhibited lower ΔE and improved L* retention compared with the HPMC-only system, suggesting that the presence of XG protected FA against chromatic degradation, which agrees with a study showing that encapsulated FA retained up to 95% of its initial luminosity L* (Das & Wong, 2020). Microencapsulation of anthocyanins using carboxymethyl starch and XG was reported to improve thermal stability, maintaining higher pigment retention and stable color over time reported by the study of Cai et al. (2019). Similar color stability was reported when XG was used with other co-pigments (e.g., rosmarinic acid), where b* shifts and ΔE were reduced significantly relative to XG-free controls (Zhao et al., 2021). Finally, XG-rich FA loaded walls confirmed better color stability under thermal storage.

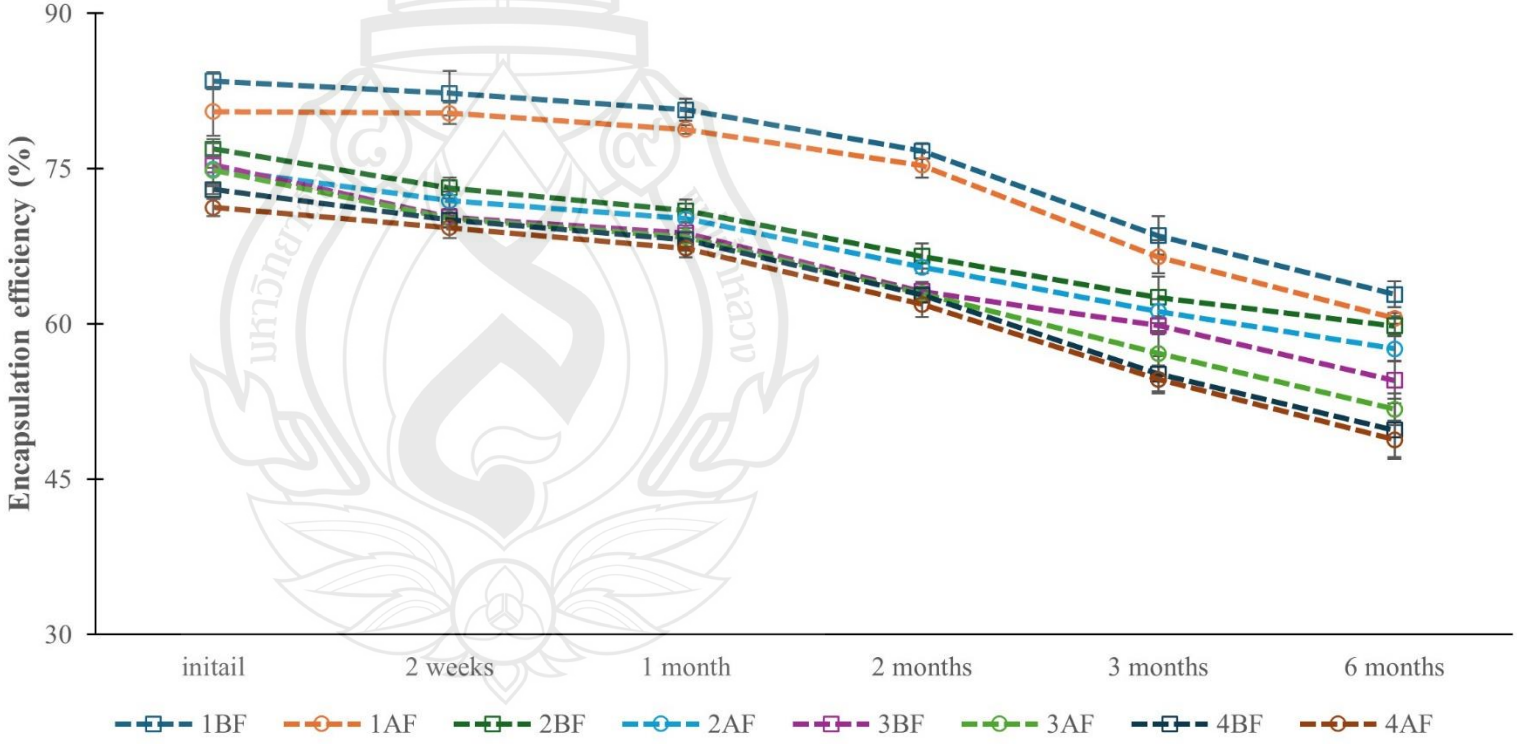

Figure 4.20 Stability of the encapsulated FA (encapsulation efficiency)

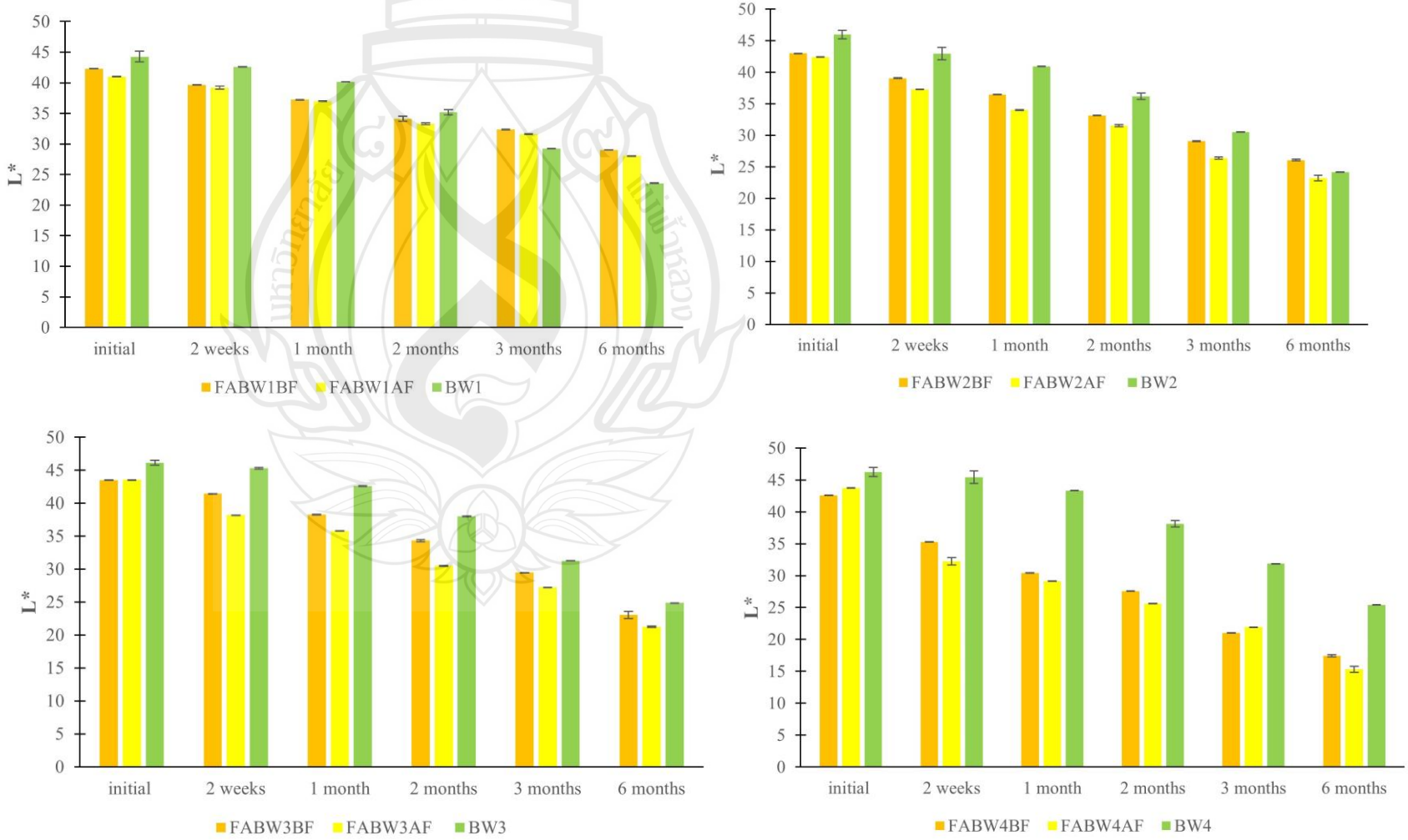

Figure 4.21 Stability of the encapsulated FA versus the biopolymeric walls (L*)

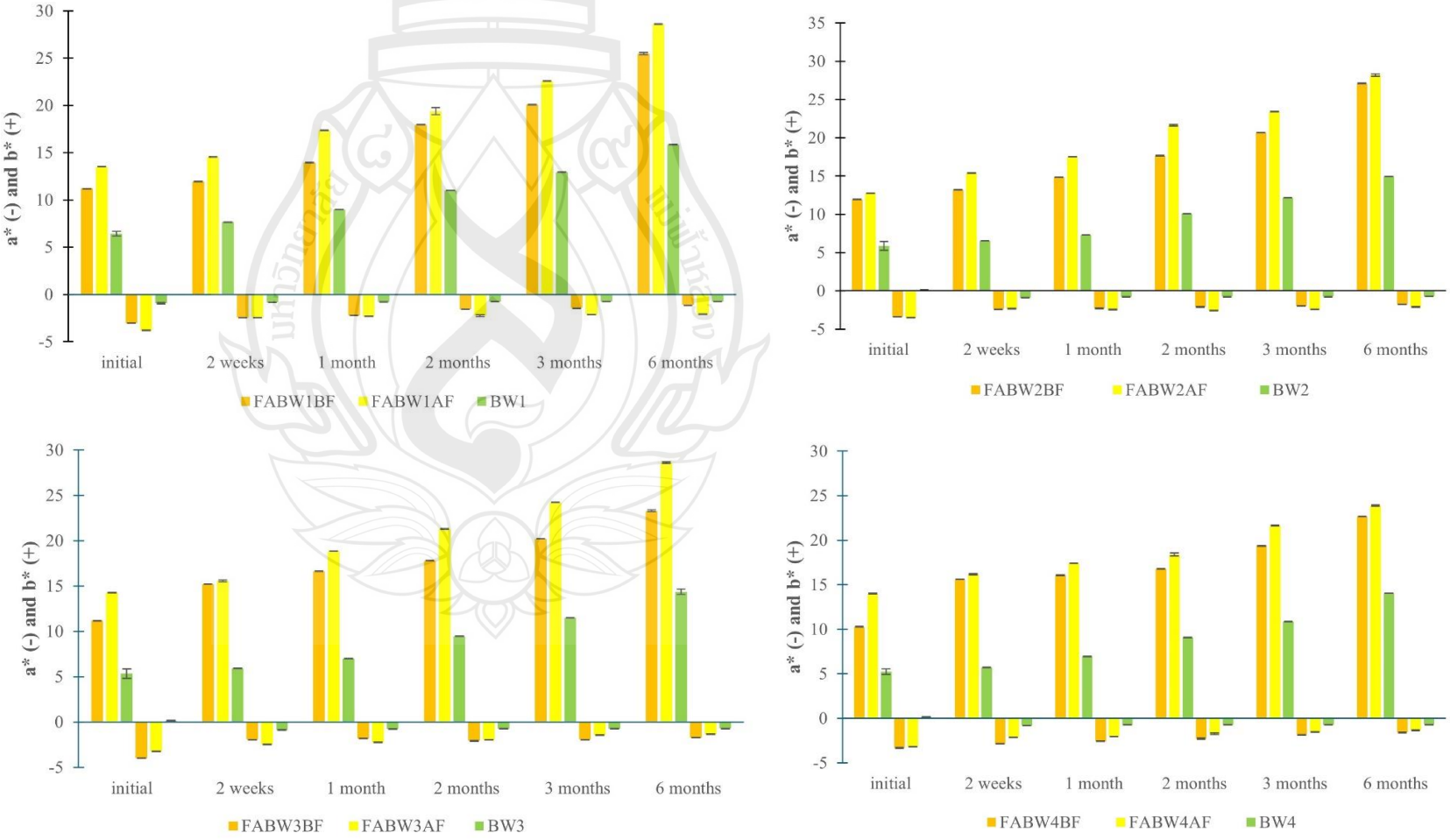

Figure 4.22 Stability of the encapsulated FA versus the biopolymeric walls (a* and b*)

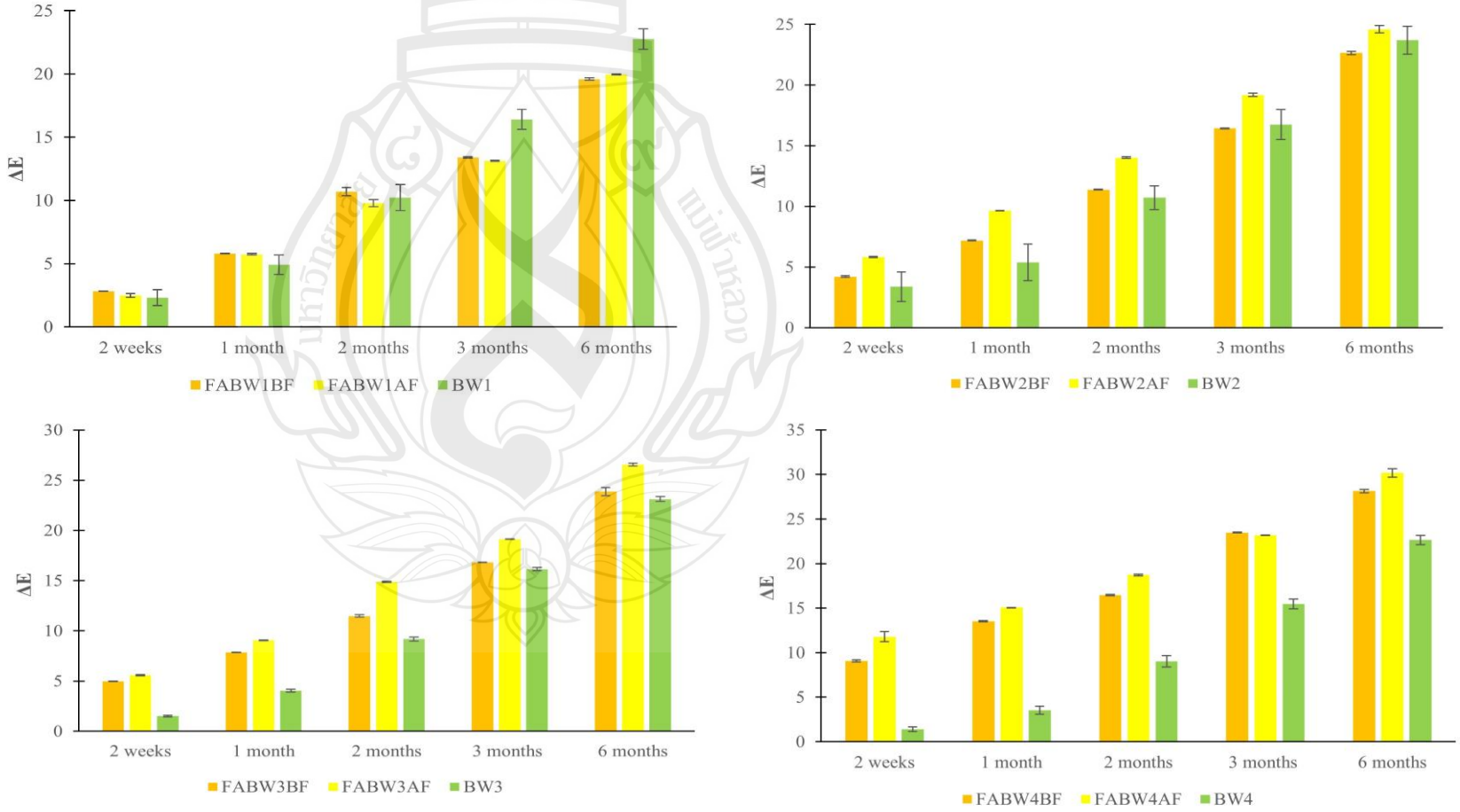

Figure 4.23 Stability of the encapsulated FA versus the biopolymeric walls (ΔE)

CHAPTER 5

CONCLUSION

This study aimed to develop and evaluate biopolymeric wall systems composing of HPMC and XG or HPMC alone for the encapsulation of ferulic acid (FA). Four biopolymeric walls formulations with varying HPMC:XG ratios; followed by eight encapsulated formulations, in which FA incorporation sequence (BF, before hydration; AF, after hydration) were comparatively evaluated.

Preparation of the biopolymeric walls by freeze-drying demonstrated that successful biopolymeric wall formation with white to off-white appearance followed by colorimetric analysis observing L* 44.26–46.25, a* 0.08–0.16, and b* 5.24–6.43. SEM, FTIR, DSC and XRD analysis revealed porous morphologies, bondings between the polymeric materials and FA, as well as amorphous structures. Physicochemical properties were evaluated, in which water solubility and absorption increased with XG due to its hydrophilic polysaccharides and porosity, but swelling capacity remained very low because of the strong gel-forming ability of HPMC, beneficial for controlled release behavior in cosmetic applications.

The encapsulation of FA in the walls was achieved and confirmed by SEM, FTIR, DSC and XRD by FA crystals into amorphous aggregate particles. Encapsulation exhibited high encapsulation efficiency (71–83%) confirming FA entrapment in the biopolymeric system. An addition of FA prior to fully hydration of the walls slightly higher in encapsulation efficacy than after fully hydrated addition.

Controlled release studies showed a sustained FA releasing over 72 h for all formulations. FA initial release within the first 6 h was relatively slow (14.66–25.31%), followed by cumulative release up to 37.97–49.07% at 72 h. AF exhibited higher cumulative releasing compared to BF, while XG contributed to higher cumulative releasing due to the swelling and viscous gel formation of XG, facilitating diffusion pathways.

Accelerated stability testing under temperature and humidity conditions of ICH guidelines revealed that encapsulated FA maintained better stability compared with free

FA. BF outperformed AF in maintaining encapsulation efficiency during stability testing and this can be attributed to the enhanced molecular dispersion of FA within the polymer during the pre-hydration, allowing better entrapment within the forming HPMC–XG system. Colorimetric stability analysis further indicated all FA-loaded walls showed gradual darkening and increased yellowness during storage; however, the presence of XG was involved in better color retention and smaller total color differences (ΔE). These findings suggest that XG contributed to improved color stability.

Overall, the findings of this study confirm that the combination of HPMC and XG can successfully fabricate a biopolymeric wall system capable of encapsulating FA, improving controlled release and stability. The enhanced stability and sustained release profile of this system supports its application into skincare formulations such as creams, serums, and masks to prolong shelf life and optimize the efficacy of FA.

Future work should focus on translating the optimized FA-loaded biopolymeric system into practical cosmetic applications such as creams, serums, and sheet masks. Future investigations are recommended to evaluate particle size distribution, zeta potential, and *in vitro* skin permeation to confirm antioxidant, photoprotective, and anti-aging benefits on human skin. Additionally, the compatibility of the encapsulated FA with other cosmetic ingredients, including emulsifiers, preservatives, and UV filters, should be explored to ensure formulation stability and product safety. Moreover, more formulation studies involving assessment of long-term stability, efficacy, and sensory properties would provide valuable insights for industrial application.

In conclusion, this study presented that HPMC and XG are the promising wall materials for the encapsulation and sustained delivery of FA to further improve its applicability in cosmetic formulations, contributing to the development of more stable antioxidant-based skincare products.

REFERENCES

Adriana, G. (2013). *Application of differential scanning calorimetry to the characterization of biopolymers*. InTech eBooks.

Afonso, T., Moresco, R., Uarrota, V. G., Navarro, B. B., Nunes, E. da C., Maraschin, M., & Rocha, M. (2017). UV-Vis and CIELAB based chemometric characterization of *Manihot esculenta* carotenoid contents. *Journal of Integrative Bioinformatics*, *14*(4), 1–13.

Ahmed, M., Akter, M. S., Lee, J. C., & Eun, J. B. (2010). Encapsulation by spray drying of bioactive components, physicochemical and morphological properties from purple sweet potato. *Food Science and Technology*, *43*(9), 1307–1312.

Akpo, E., Colin, C., Perrin, A., Cambedouzou, J., & Cornu, D. (2024). Encapsulation of active substances in natural polymer coatings. *Materials*, *17*(11), 2774.

Ammala, A. (2013). Biodegradable polymers as encapsulation materials for cosmetics and personal care markets. *International Journal of Cosmetic Science*, *35*(2), 113–206.

Banerjee, S., Chattopadhyay, P., Ghosh, A., Bhattacharya, S. S., Kundu, A., & Veer, V. (2014). Accelerated stability testing of a transdermal patch composed of eserine and pralidoxime chloride for prophylaxis against (±)-anatoxin a poisoning. *Journal of Food and Drug Analysis*, *22*(2), 264–270.

Bhansali, M., Dabholkar, N., Swetha, P., Dubey, S. K., & Singhvi, G. (2021). *Solid oral controlled-release formulations*. Elsevier eBooks.

Blanco, I., & Siracusa, V. (2021). The use of thermal techniques in the characterization of bio-sourced polymers. *Materials, 14*(7), 1–20.

Cai, X., Du, X., Cui, D., Wang, X., Yang, Z., & Zhu, G. (2019). Improvement of stability of blueberry anthocyanins by carboxymethyl starch/xanthan gum combinations microencapsulation. *Food Hydrocolloids*, *91*, 238–245.

Casanova, F., & Santos, L. (2016). Encapsulation of cosmetic active ingredients for topical application. A review. *Journal of Microencapsulation, 33*(1), *1*–17.

Cavalcanti, G. R., Duarte, F. I. C., Converti, A., & de Lima, Á. A. N. (2020). Ferulic acid activity in topical formulations: technological and scientific prospecting. *Current Pharmaceutical Design*, *27*(19), 2289–2298.

Chaturvedi, S., Kulshrestha, S., Bhardwaj, K., & Jangir, R. (2021). A review on properties and applications of xanthan gum. *Microbial Polymers: Applications and Ecological Perspectives*, 87–107.

Chen, L., Ming, Z., Li, W., Zhou, Y., Zhang, S., Yang, X., Xin, J., & Zhang, N. (2025). OSA-modification rice, debranched, and soluble starches encapsulating ferulic acid: interfacial effects, solubility, stability, bioactivity, and sustained release. *International Journal of Biological Macromolecules*, *334*(2), 149163.

Costa, A. M. M., Moretti, L. K., Simões, G., Silva, K. A., Calado, V., Tonon, R. V., & Torres, A. G. (2020). Microencapsulation of pomegranate (*Punica granatum L.*) seed oil by complex coacervation: Development of a potential functional ingredient for food application. *LWT*, *131*(20), 109519.

Das, S., & Wong, A. B. H. (2020). Stabilization of ferulic acid in topical gel formulation via nanoencapsulation and pH optimization. *Scientific Reports*, *10*(1), 12288.

Dave, P. N., & Gor, A. (2018). Natural polysaccharide-based hydrogels and nanomaterials. *Handbook of Nanomaterials for Industrial Applications*. (pp. 36–66). Elsevier.

Deshmukh, K., Basheer Ahamed, M., Deshmukh, R. R., Khadheer Pasha, S. K., Bhagat, P. R., & Chidambaram, K. (2017). Biopolymer composites with high dielectric performance: interface engineering. *Biopolymer Composites in Electronics*, Elsevier, 27–128.

Fara, D. A., Dadou, S. M., Rashid, I., Al-Obeidi, R., Antonijevic, M. D., Chowdhry, B. Z., & Badwan, A. (2019). A direct compression matrix made from xanthan gum and low molecular weight chitosan designed to improve compressibility in controlled release tablets. *Pharmaceutics*, *11*(11), 1–24.

Fonseca, L. M., Halal, S. L. M. El, Dias, A. R. G., & Zavareze, E. da R. (2021). Physical modification of starch by heat-moisture treatment and annealing and their applications. A review. *Carbohydrate Polymers*, *274,* 118665.

Ford, J. L. (1999). Thermal analysis of hydroxypropyl methylcellulose and methylcellulose: Powders, gels and matrix tablets. *International Journal of Pharmaceutics*, *179*(2), 209–228.

Gao, R., Zhao, D., Zhou, X., Wan, Z., Wang, X., Rao, H., . . . Hao, J. (2025). Advances in polysaccharide-based biopolymers for probiotic encapsulation: from single polysaccharides to composite systems. *Current Research in Food Science*, *11*, 1–17.

Guo, Q. (2016). *Polymer Morphology: Principles, Characterization, and Processing*. Wiley eBooks.

Gupta, K. M., Das, S., Chow, P. S., & Macbeath, C. (2020). Encapsulation of ferulic acid in lipid nanoparticles as antioxidant for skin: mechanistic understanding through experiment and molecular simulation. *ACS Applied Nano Materials*, *3*(6), 5351–5361.

Harasym, J., Satta, E., & Kaim, U. (2020). Ultrasound treatment of buckwheat grains impacts important functional properties of flour. *Molecules*, *25*(13), 3012.

Jaiturong, P., Laosirisathian, N., Sirithunyalug, B., Eitssayeam, S., Sirilun, S., Chaiyana, W., & Sirithunyalug, J. (2020). Physicochemical and prebiotic properties of resistant starch from *Musa sapientum* Linn., ABB group, cv. Kluai Namwa Luang. *Heliyon*, *6*(12), e05789.

Jang, Y., & Koh, E. (2023). Characterisation and storage stability of aronia anthocyanins encapsulated with combinations of maltodextrin with carboxymethyl cellulose, gum Arabic, and xanthan gum. *Food Chemistry*, *405*(23), 135002.

Jayadev, S., & Ismail, Y. (2023). A review on *in-vitro* release testing methods for topical dosage forms. *Journal of Drug and Alcohol Research*, *12*(11), 236274.

Kouassi, M. C., Grisel, M., & Gore, E. (2022). Multifunctional active ingredient-based delivery systems for skincare formulations: A review. *Colloids and Surfaces B: Biointerfaces*, 217, 1–53.

Lin, F. H., Lin, J. Y., Gupta, R. D., Tournas, J. A., Burch, J. A., Selim, M. A., . . . Pinnell, S. R. (2005). Ferulic acid stabilizes a solution of vitamins C and E and doubles its photoprotection of skin. *Journal of Investigative Dermatology*, *125*(4), 826–832.

Lukas, K., & LeMaire, P. K. (2009). Differential scanning calorimetry: fundamental overview. *Resonance*, *14*(8), 807-817.

Mahdavi, S., Jafari, S. M., Assadpoor, E., & Dehnad, D. (2016). Microencapsulation optimization of natural anthocyanins with maltodextrin, gum Arabic and gelatin. *International Journal of Biological Macromolecules*, *85*, 379–385.

Mandal, P., Purushottam, K. A., Shekhar, N., Srivastava, A., Jaiswal, S., Bharty, M. K., & Kumar, R. (2025). Temperature-tunable adsorption of methylene blue by Poly (AAC-Co-AAM) hydrogels: swelling behavior, kinetics, and isotherm studies. *Journal of Applied Polymer Science*, *142*(42), e57626.

Manian, M., Jain, P., Vora, D., & Banga, A. K. (2022). Formulation and evaluation of the *in vitro* performance of topical dermatological products containing diclofenac sodium. *Pharmaceutics*, *14*(9),1892.

Mendoza-Muñoz, N., Leyva-Gómez, G., Piñón-Segundo, E., Zambrano-Zaragoza, M. L., Quintanar-Guerrero, D., Del Prado Audelo, M. L., & Urbán-Morlán, Z. (2023). Trends in biopolymer science applied to cosmetics. *International Journal of Cosmetic Science*, *45*(6), 699-724.

Min, R. (2025). Chemical stability of cosmetic ingredients: mechanisms of degradation and influencing factors. *Applied and Computational Engineering*, *156*(1), 35-40.

Mitura, S., Sionkowska, A., & Jaiswal, A. (2020). Biopolymers for hydrogels in cosmetics: A review. *Journal of Materials Science*, *31*(6), 50.

Mota, L. B., da Silva Campelo, M., de Almeida Silva, G., de Oliveira, C. L. C. G., Gramosa, N. V., Ricardo, N. M. P. S., & Ribeiro, M. E. N. P. (2022). Spectrophotometric method for quantification of eugenol in volatile oil of clove buds and nanoemulsion. *Revista Brasileira de Farmacognosia*, *32*(6), 912–920.

Mudalip, S. K., Khatiman, M. N., Hashim, N. A., Che Man, R., & Arshad, Z. I. M. (2019). A short review on encapsulation of bioactive compounds using different drying techniques. *Materials Today: Proceedings*, *42*(1), 288–296.

Mughal, M. A., Iqbal, Z., & Neau, S. H. (2011). Guar gum, xanthan gum, and HPMC can define release mechanisms and sustain release of propranolol hydrochloride. *AAPS PharmSciTech*, *12*(1), 77–87.

Naeem, A., Yu, C., Zang, Z., Zhu, W., Deng, X., & Guan, Y. (2023). Synthesis and evaluation of rutin–hydroxypropyl β-cyclodextrin inclusion complexes embedded in xanthan gum-based (HPMC-g-AMPS) hydrogels for oral controlled drug delivery. *Antioxidants*, *12*(3), 552.

Navarro-Flores, M. J., Ventura-Canseco, L. M. C., Meza-Gordillo, R., Ayora-Talavera, T. del R., & Abud-Archila, M. (2020). Spray drying encapsulation of a native plant extract rich in phenolic compounds with combinations of maltodextrin and non-conventional wall materials. *Journal of Food Science and Technology*, *57*(11), 4111–4122.

Ng, J. Y., Obuobi, S., Chua, M. L., Zhang, C., Hong, S., Kumar, Y., Gokhale, R., & Ee, P. L. R. (2020). Biomimicry of microbial polysaccharide hydrogels for tissue engineering and regenerative medicine. A review. *Carbohydrate Polymers*, *241*, 116345.

Noorlaila, A., Hasanah, H. N., Yusoff, A., Sarijo, S. H., & Asmeda, R. (2017). Effects of xanthan gum and HPMC on physicochemical and microstructure properties of sponge cakes during storage. *Journal of Food Science and Technology*, *54*(11), 3532–3542.

Ozkan, G., Franco, P., De Marco, I., Xiao, J., & Capanoglu, E. (2019). A review of microencapsulation methods for food antioxidants: Principles, advantages, drawbacks and applications. *Food Chemistry*, *272*(30), 494-506.

Palanikumar, L., Choi, E. S., Oh, J. Y., Park, S. A., Choi, H., Kim, K., Kim, C., & Ryu, J. H. (2018). Importance of encapsulation stability of nanocarriers with high drug loading capacity for increasing *in vivo* therapeutic efficacy. *Biomacromolecules*, *19*(7), 3030-3039.

Patkowska, S., Cichy, M., & Flieger, J. (2025). Application of Fourier Transform Infrared (FTIR) spectroscopy in characterization of green synthesized nanoparticles. *Molecules*, *30*(3), 1–36.

Pattnaik, S., Barik, S., Muralitharan, G., & Busi, S. (2018). Ferulic acid encapsulated chitosan-tripolyphosphate nanoparticles attenuate quorum sensing regulated virulence and biofilm formation in pseudomonas aeruginosa PAO1. *IET Nanobiotechnology*, *12*(8), 1056–1061.

Paul, S., Sahu, M., Mandal, P., Quraishi, A., & Dixit, S. (2022). A peer review of xanthan gum derivatives in development of drug delivery systems. *Journal of Emerging Technologies and Innovative Research, 9*(4), 342-368.

Petrișor, G., Motelica, L., Ficai, D., Ilie, C. I., Trușcă, R. D., Surdu, V. A., . . . Dițu, L. M. (2023). Increasing bioavailability of trans-ferulic acid by encapsulation in functionalized mesoporous silica. *Pharmaceutics*, *15*(2), 1-19.

Pueknang, J., & Saewan, N. (2022). Stability and anti-aging of encapsulated ferulic acid in phosphorylated rice starch. *Molecules*, *27*(11), 1-19.

Purushothaman, J. R., & Rizwanullah, Md. (2024). Ferulic Acid: A Comprehensive Review. *Cureus*. *16*(8), e68063.

Rezagholizade-Shirvan, A., Soltani, M., Shokri, S., Radfar, R., Arab, M., & Shamloo, E. (2024). Bioactive compound encapsulation: characteristics, applications in food systems, and implications for human health. *Food Chemistry*, *24*, 101953.

Rezvankhah, A., Emam-Djomeh, Z., & Askari, G. (2020). Encapsulation and delivery of bioactive compounds using spray and freeze-drying techniques: A review. *Drying Technology*, *38*(1–2), 235-258.

Romeo, A., Musumeci, T., Carbone, C., Bonaccorso, A., Corvo, S., Lupo, G., . . . Pignatello, R. (2021). Ferulic acid-loaded polymeric nanoparticles for potential ocular delivery. *Pharmaceutics*, *13*(5), 1-19.

Sajjadi, S. E., Shokoohinia, Y., & Moayedi, N. S. (2012). Isolation and identification of ferulic acid from aerial parts of *Kelussia odoratissima* mozaff. *Journal of Natural Pharmaceutical Products*, *7*(4), 159-162.

Schantz, L., Schagerlöf, H., Karlsson, E. N., & Ohlin, M. (2014). Characterization of the substitution pattern of cellulose derivatives using carbohydrate-binding modules. *BMC Biotechnology*, *14*(1), 1–8.

Shen, J., & Burgess, D. J. (2013). *In vitro* dissolution testing strategies for nanoparticulate drug delivery systems: Recent developments and challenges. *Drug Delivery and Translational Research*, *3*(5), 409-415.

Shukla, D., Nandi, N. K., Singh, B., Singh, A., Kumar, B., Narang, R. K., & Singh, C. (2022). Ferulic acid-loaded drug delivery systems for biomedical applications. *Journal of Drug Delivery Science and Technology*, *75(2)*, 103621.

Sowmya, C., Kumar, V. L., & Adhikari, B. (2022). Optimization and analysis of xanthan gum and hypromellose combined matrices for extended release of ranolazine using quality by design. *International Journal of Pharmaceutical Investigation*, *12*(1), 87-92.

Suksaeree, J., Monton, C., Madaka, F., Chusut, T., Saingam, W., Pichayakorn, W., & Boonme, P. (2014). Formulation, physicochemical characterization, and *in vitro* study of chitosan/HPMC blends-based herbal blended patches. *AAPS PharmSciTech*, *16*(1), 171–181.

Sweed, N. M., Dawoud, M. H. S., Aborehab, N. M., & Ezzat, S. M. (2024). An approach for an enhanced anticancer activity of ferulic acid-loaded polymeric micelles via MicroRNA-221 mediated activation of TP53INP1 in caco-2 cell line. *Scientific Reports*, *14*(1), 2073.

Torres-Perez, R., Martínez-García, E., Igual, M., Martínez-Monzó, J., & García-Segovia, P. (2023). Effect of hydroxypropyl methylcellulose, xanthan gum, and psyllium in the formulation of gluten-free bread for the improvement of organoleptic quality. *Foods, 26*(1), 48.

Velázquez, D. A. (2025). Ferulic acid: mechanistic insights and multifaceted applications in metabolic syndrome, food preservation, and cosmetics. *Molecules*, *30*(18), 1–38.

Venkateshaiah, A., Padil, V. V. T., Nagalakshmaiah, M., Waclawek, S., Černík, M., & Varma, R. S. (2020). Microscopic techniques for the analysis of micro and nanostructures of biopolymers and their derivatives. *Polymers*, *12*(3), 512.

Venkateswarlu, K. (2017). Evaluation of glibenclamide microspheres for sustained release. *Journal of Pharmacy and Pharmacognosy Research*, *5*(2), 78-87.

Vierkötter, A., & Krutmann, J. (2012). Environmental influences on skin aging and ethnic-specific manifestations. *Dermato-Endocrinology*, *4*(3), 227-231.

Vlad, R. A., Pintea, A., Pintea, C., Rédai, E. M., Antonoaea, P., Bîrsan, M., & Ciurba, A. (2025). Hydroxypropyl methylcellulose—a key excipient in pharmaceutical drug delivery systems. *Pharmaceutics, 17*(6), 1-30.

Wan, S., Dai, C., Bai, Y., Xie, W., Guan, T., Sun, H., & Wang, B. (2021). Application of multivariate methods to evaluate differential material attributes of HPMC from different sources. *ACS Omega*, *6*(43), 28598-28610.

Wang, J., Cao, Y., Sun, B., & Wang, C. (2011). Characterisation of inclusion complex of trans-ferulic acid and hydroxypropyl-β-cyclodextrin. *Food Chemistry*, *124*(3), 1069–1075.

Wang, N., Wang, B., Wan, Y., Gao, B., & Rajput, V. D. (2023). Alginate-based composites as novel soil conditioners for sustainable applications in agriculture: A critical review. *Journal of Environmental Management*, *348*, 119133.

Weatherall, I. L., & Coombs, B. D. (1992). Skin color measurements in terms of CIELAB color values. *Journal of Investigative Dermatology*, *99*(4), 468-473.

Yadav, H., & Karthikeyan, C. (2019). Natural polysaccharides: Structural features and properties. *Polysaccharide Carriers for Drug Delivery*, (pp.1-17). Elsevier.

Yu, J. Y., Roh, S. H., & Park, H. J. (2021). Characterization of ferulic acid encapsulation complexes with maltodextrin and hydroxypropyl methylcellulose. *Food Hydrocolloids*, *111*(2), 106390.

Zduńska, K., Dana, A., Kolodziejczak, A., & Rotsztejn, H. (2018). Antioxidant properties of ferulic acid and its possible application. *Skin Pharmacology and Physiology*, *31*(6), 332-336.

Zhao, L., Pan, F., Mehmood, A., Zhang, H., Rehman, A. U., Li, J., . . . Wang, C. (2021). Improved color stability of anthocyanins in the presence of ascorbic acid with the combination of rosmarinic acid and xanthan gum. *Food Chemistry*, 351, 129317.

Zheng, M., Chen, J., Tan, K. B., Chen, M., & Zhu, Y. (2022). Development of hydroxypropyl methylcellulose film with xanthan gum and its application as an excellent food packaging biomaterial in enhancing the shelf life of banana. *Food Chemistry*, *374*(16), 131794.

Zhou, C., Shi, X., Wang, H., & An, N. (2007). Measurement and correlation of solubilities of trans-ferulic acid in solvents. *Huagong Xuebao/Journal of Chemical Industry and Engineering (China)*, *58*(11), 2705-2709.

APPENDIX A

UV-VIS ANALYSIS

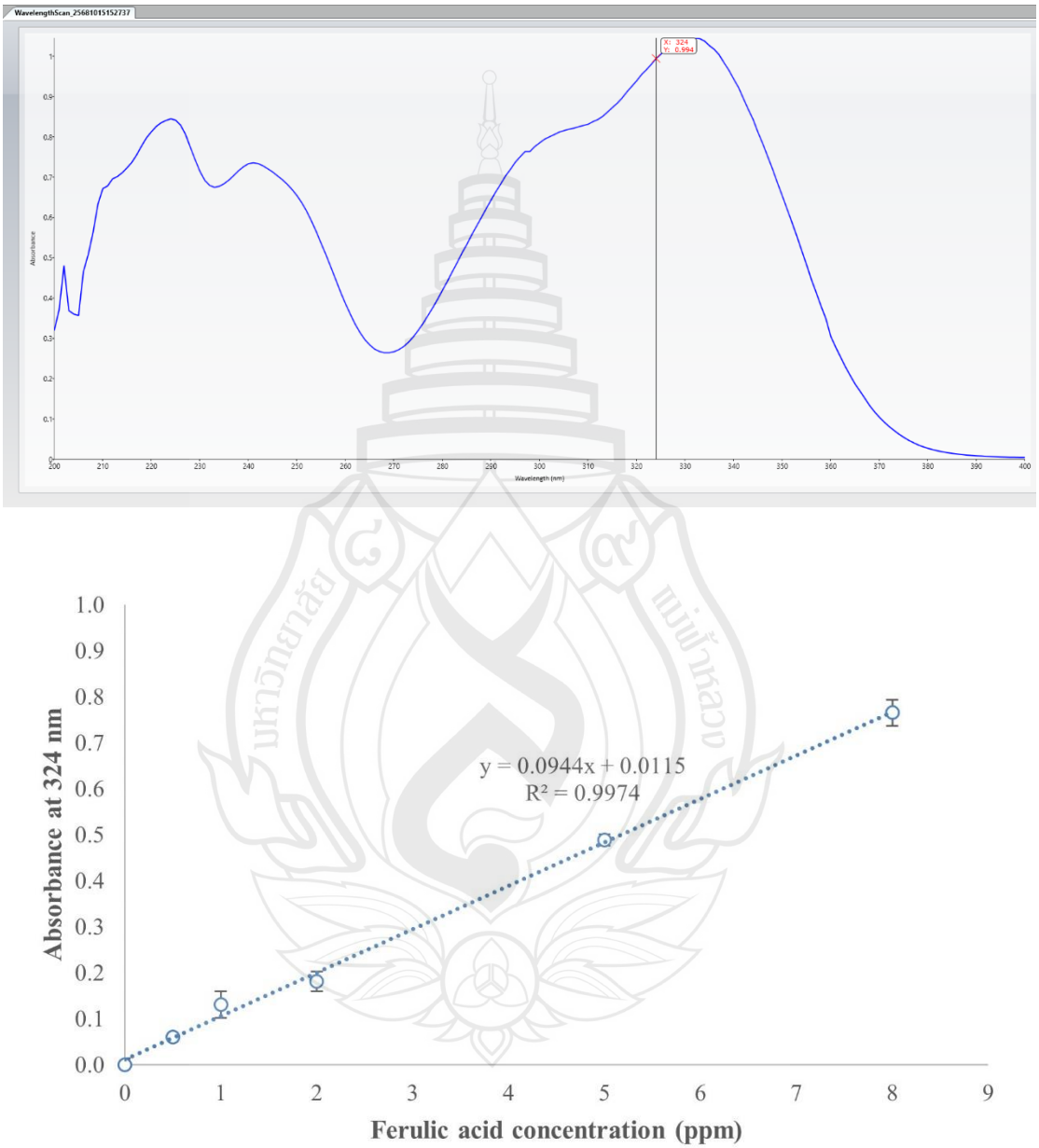

Figure A1 UV-Vis wavelength scan and calibration curve of ferulic acid standard

APPENDIX B

CERTIFICATE OF ORAL PRESENTATION AWARD

Figure B1 Certificate of oral presentation award at PACCON 2026

APPENDIX C

PROCEEDING

No.70 FA-O-07

Fabrication of Biopolymeric Walls for Ferulic Acid Encapsulation

Zaw Myo Htet[1], Nattaya Lourith[1,2]*
[1]*School of Cosmetic Science, Mae Fah Luang University, Chiang Rai 57100, Thailand*
[2]*Phytocosmetics and Cosmeceutical Research Group, Mae Fah Luang University, Chiang Rai 57100, Thailand*
**E-mail: nattayal@mfu.ac.th*

Abstract:

Ferulic acid (FA) is a phenolic compound widely used in cosmetics due to its pharmacological properties; however, its instability limits its applications. This study aimed to fabricate biopolymeric walls for FA encapsulation using hydroxypropyl methylcellulose (HPMC) and xanthan gum (XG) at ratios (50:1 to 250:1 w/w). The fabricated microspheres were exhibited by SEM with pore sizes between 37-51 µm (ImageJ). FTIR spectra indicated bonding between HPMC and XG through characteristic O–H (3423 cm^{-1}), C=O (1690 cm^{-1}), and C–O–C (1051 cm^{-1}) bands. DSC demonstrated the improved thermal characteristics. XRD confirmed favorable amorphous structure following reductions in HPMC diffractions. The biopolymeric walls were thereafter FA (2% w/w loading) with an encapsulation efficiency of FA (75.41 ± 3.82 %). FTIR and SEM confirmed the encapsulation. The FA loaded walls improved in thermal stability, whereby its melting temperature (174.86 ± 2.66°C) was undetected in DSC. In addition, XRD indicated the amorphous FA (2θ of 8.98°-17.38°) associates in the improved thermal stability. Moreover, FA encapsulations in the fabricated biopolymeric walls were exhibited to be improved in water solubility (from 30-38% to 34-40%), water absorption (from 16-18% to 17-25%) and swelling index (from 4-6 $\times 10^{-3}$% to 5-7 $\times 10^{-3}$%), favoring cosmetic formulation practices.

1. Introduction

Ferulic acid (FA) is a phenolic compound with potent antioxidants, anti-inflammatory, and anti-aging properties, making it a preferred active ingredient in cosmetic formulations. When applied topically, FA shows photoprotective effects, reduces hyperpigmentation, improves skin elasticity, and enhances overall skin texture.[1] Despite its therapeutic potential, FA faces stability challenges that limit cosmetic applications. One of the methods to prolong FA stability and solubility is encapsulation, which protects the active within a polymer wall matrix from external factors while preserving its bioactivity until applications. A study of microencapsulation using maltodextrin and hydroxypropyl methylcellulose was reported to improve FA stability.[2]

A wide range of natural and synthetic wall materials have been used for encapsulation, based on their functional performances which include polysaccharides (alginate, chitosan, starch, cellulose derivatives, xanthan gum), and proteins (gelatin, whey protein, zein) are the commonly used polymers for wall fabrication. Biopolymers can swell, dissolve, or break down on specific skin conditions; and biopolymer-based encapsulations are widely used because of being non-toxic, biodegradability, cost-effective and easily modified.[3] They are well known for their physical properties including solubility, temperature stability, mechanical stability, and thickening.[4]

Hydroxypropyl methylcellulose (HPMC), a semi-synthetic cellulose derivative recognized for its high film-forming ability which creates a protective physical barrier around bioactive compounds by reducing oxygen and moisture permeability, preventing degradation. Xanthan gum (XG), an anionic natural polysaccharide contributes rapid hydration, high viscosity at low concentrations, biocompatibility, and heat stability properties. The combination of HPMC and XG creates a complementary carrier: which has been shown overcoming individual polymer limitations, achieving release kinetics and enhanced encapsulation efficiency.[5]

Therefore, the aim of this research is to fabricate biopolymeric walls for FA encapsulation, evaluating its characteristics, physicochemical properties, and encapsulation efficiency to feature its potential as an effective delivery system for cosmetic applications.

2. Materials and Methods

2.1 Materials

The chemicals used in this study were ferulic acid (Fisher Scientific, UK), hydroxypropyl methylcellulose HPMC (Sigma, cosmetic grade, Singapore), and xanthan gum (MySkinRecipes, USA). All other reagents were of analytical grade. Reverse osmosis water (RO + alkaline system using sediment and carbon filters, 0.0001 µm RO membrane, and an alkaline carbon block) was used

for encapsulation while deionized water (Progard TS2 system and Millipak® 0.22 µm filter) was used for analytical characterization.

2.2 Preparation of biopolymeric walls and FA loaded walls

Biopolymeric walls were prepared by the modified methods using HPMC:XG (50:1 to 250:1 w/w).[6,7] The walls were prepared by dissolving HPMC in RO water followed by XG. The mixtures were hydrated at 4 °C for 24 h, and lyophilized. The walls were loaded with FA (2% w/w).[8]

Table 1. Composition of formulations (% w/w)

Code	FA	HPMC:XG	Description
BW1	–	50:1	Blank wall 1
BW2	–	125:1	Blank wall 2
BW3	–	250:1	Blank wall 3
BW4	–	HPMC only	Blank wall 4
FABW1	2%	50:1	FA-loaded wall 1
FABW2	2%	125:1	FA-loaded wall 2
FABW3	2%	250:1	FA-loaded wall 3
FABW4	2%	HPMC only	FA-loaded wall 4

2.3 Characterizations of biopolymeric walls and FA loaded walls

BW and FABW were characterized by SEM (MIRA, TESCAN, Czech Republic), FTIR ATR (Nicolet iS50, Thermo Fisher Scientific, USA), DSC (DSC 3+, METTLER TOLEDO, USA) and XRD (Empyrean, PANalytical, UK).[2]

2.4 Physicochemical properties of biopolymeric walls and FA loaded walls

BW and FABW were determined in their water solubility index (WSI), water absorption rate (WAR), and swelling capacity (SC) by the modified method.[9] The sample (25 mg in 10 mL of DI water) was centrifuged, the supernatant was collected and dried. Experiments were done in triplicate and WSI, WAR, and SC were calculated.

$$\text{WSI} = \frac{\text{Supernatant dried weight}}{\text{Initial weight microcapsules}} \times 100$$

$$\text{WAR} = \frac{\text{Fresh sediment weight}}{\text{Initial weight microcapsules}}$$

$$\text{SC} = \frac{\text{Supernatant dried weight}}{\text{Initial weight microcapsules} \times (100\text{-WSI})}$$

2.5 Encapsulation efficiency

Encapsulation efficiency (EE) was quantified using a previously reported method.[2] FABW (10 ppm in methanol, prepared from 1000 ppm stock) were sonicated (Crest 690DAE ultrasonic bath, 50/60 Hz, power level 4, 10 min), centrifuged (Mether DL-3020HR, 9000 rpm, 10 min), and analyzed via UV-Vis spectrophotometer (Biochrom, Libra S80) at 324 nm. Concentrations were calculated from FA's calibration curve (R^2 = 0.9974, 0.5–8 ppm). Experiments were performed in triplicate, with EE calculated as follows.

$$\text{EE (\%)} = \frac{\text{Weight of FA loaded - weight of free FA}}{\text{Weight of FA loaded}} \times 100$$

2.6 Statistical Analysis

All experiments were conducted in triplicates and data were shown as mean ± standard deviation for each experiment. Statistical analyses were conducted using SPSS software (SPSS 20.0, IBM, Chicago, IL). One-way analysis of variance (ANOVA) and Tukey tests were executed at 95% confidence level to assess significant differences.

3. Results & Discussion

3.1 Preparation of biopolymeric walls and FA loaded walls

Four biopolymeric walls (79.74 -73.60 % yield) and four FA loaded walls (76.24 – 64.35 % yield) were prepared. BW appeared as very white, light solids while FABW were seen as pale yellow, larger solids with smooth surfaces.

3.2 Characterizations of biopolymeric walls and FA loaded walls

The morphological characteristics of BW, HPMC and XG were studied by using SEM and pore sizes were determined by ImageJ. HPMC illustrated irregular, fibrous morphology with elongated layers showing wrinkling and folding.[10] XG showed granular morphology with rough surfaces and visible flakes.[11] BW appeared off white to the naked eye due to their high surface area and light scattering from the porous network. In Table 2, the pore sizes of the walls ranged from 37.16 to 51.49 µm, with porosity increasing with higher XG content. However, pores were reduced and partially collapsed after FA was loaded. This may be attributed to the presence of FA within the wall, where FA particles could occupy the surface pores, resulting in a more compact and less porous appearance as observed in Figure 1. Additionally, FA loading may promote polymer–FA interactions as evidenced by FTIR, thereby reducing the visibility of pores in SEM images. This suggested that FABW was occupied with FA amorphous aggregates and loss of FA original morphology.[2]

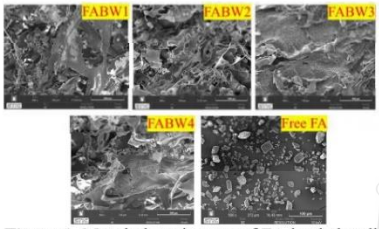

Figure 1. Morphology images of FA loaded walls (FABW) and free FA under 500x magnification.

FTIR confirmed biopolymeric walls and the successful encapsulation of FA (Figure 2). The BW spectra displayed a broad O–H stretching (3430 cm^{-1}), C–H stretching (2918 cm^{-1}), XG carboxylate peaks (1645, 1454, 1375 cm^{-1}), and strong polysaccharide C–O–C vibrations (1051 cm^{-1}), indicating a hydrogen-bonded HPMC–XG matrix. Free FA showed characteristic O–H (3432 cm^{-1}), C=O (1688 cm^{-1}), aromatic C=C (1618–1431 cm^{-1}), C–O–C (1266 cm^{-1}) and out of plane aromatic C–H peaks at 851–803 cm^{-1}.[12]

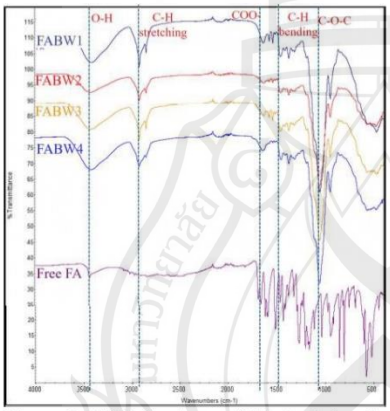

Figure 2. FTIR Spectrum of FA loaded walls (FABW) and free FA.

FA encapsulation can be confirmed through: (1) O–H broadening at 3420 cm^{-1}, (2) retention of biopolymeric walls (C–H at 2918 cm^{-1} and C–O–C at 1051 cm^{-1}), (3) shifted peaks of COO^- at 1619 cm^{-1} where the phenolic hydrogen of FA bonds to the carboxylate oxygen of XG, and (4) disappearance of FA characteristic peaks in 1690 cm^{-1} to 1660 cm^{-1}, where the absence of doublet peak of FA carboxylic acid carbonyl (C=O) means FA lost its crystalline form. Similar trends were observed in 1517 cm^{-1} for aromatic ring vibration and 1277 cm^{-1} for phenolic C–O stretch.

DSC confirmed FA encapsulation through significant thermal profiles (Figure 3). HPMC and XG exhibited broad water-loss peaks at 84.9°C and 92.7°C respectively, while biopolymeric walls showed broad endothermic peaks with decreased melting temperatures (T_m) as shown in Table 1. Free FA displayed a single sharp endothermic melting peak at 174°C, corresponding to thermal decomposition at higher temperatures, however, this peak completely disappeared when FA was loaded.[13] Significant difference ($p<0.05$) is observed across the range (73.37-79.89°C), with the lowest temperature in FABW1 being significantly different from the highest FABW4. The enhancement of FA stability is evidenced by the disappearance of the FA melting endotherm (174.86°C) in DSC thermograms of FABW. This lack of a detectable melting endotherm confirms that the biopolymeric walls prevent the thermal decomposition of FA at its melting temperature, thereby improving its thermal stability.

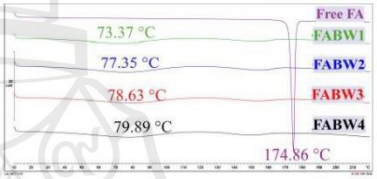

Figure 3. DSC thermograms of FA loaded walls (FABW) and Free FA

Table 2. Key parameters of formulations

Sample	Pore size (μm)	T_m (°C)
BW1	51.49 ± 2.85^{a}	$82.95 \pm 4.02^{c,d,e}$
BW2	44.05 ± 1.35^{b}	$82.72 \pm 2.04^{c,d,e}$
BW3	$41.71 \pm 2.13^{b,c}$	$82.28 \pm 1.45^{c,d,e}$
BW4	37.16 ± 0.86^{c}	$83.39 \pm 1.62^{c,d,e}$
HPMC	n.d.	$84.89 \pm 4.00^{d,e}$
XG	n.d.	92.67 ± 0.78^{f}
FABW1	n.d.	73.37 ± 1.09^{a}
FABW2	n.d.	77.35 ± 0.93^{b}
FABW3	n.d.	$78.63 \pm 1.91^{b,c}$
FABW4	n.d.	$79.89 \pm 2.09^{b,c,d}$
Free FA	n.d.	174.86 ± 2.66^{g}

T_m= melting temperature; n.d.= not detected; Values are given as mean ± S.D. Different letters in the same column are significantly different ($p < 0.05$).

XRD confirmed FA encapsulation by changes in peak intensity and crystallinity of the

biopolymeric wall after loading FA (Figure 4). Pure HPMC exhibited two amorphous peaks at 2θ 8.1° and 20.46°, corresponding to its semi-crystalline structure, while XG displayed a broad halo at 8.0° and 19.72°. Biopolymeric walls showed a progressive reduction of diffraction peaks intensity at 2θ (10.14°–19.85°), indicating decreased crystallinity due to strong hydrogen bonding, and enhanced amorphous character. Free FA showed strong crystalline characteristics with sharp peaks at 2θ (9.00°, 10.54°, 12.81°, 15.73°, 17.44°, 26.48°), while FA loaded walls exhibited reduced crystallinity, in 20°–30°, confirming successful encapsulation of FA within the walls because its diffraction pattern was clearly distinguished from individual component, showing changes from crystalline to amorphous form.[14] The structural stability of FA is confirmed by the loss of FA crystalline diffraction peaks beyond 2θ of 20°, some of which are significantly reduced. The new broad amorphous halo indicates that FA molecules are already dispersed within the walls, preventing from recrystallization.

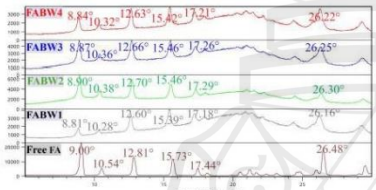

Figure 4. X-ray diffraction patterns of FA loaded walls (FABW) and free FA.

3.3 Physicochemical properties of biopolymeric walls and FA loaded walls

The physicochemical properties were significantly influenced by the interaction between HPMC and XG (Figure 5). Pure HPMC and XG showed higher WSI 75.65 % and 71.94 % respectively whereas biopolymeric walls exhibited lower WSI due to HPMC's gel forming ability, limiting immediate water dissolution with XG. Biopolymeric walls with higher XG showed higher WSI and WAR due to XG's anionic nature, enabling its carboxylate groups (–COO^-) to form hydrogen bonding that facilitate water absorption.[5] Swelling capacity was influenced by HPMC's gel-forming characteristics (SC: 0.032) compared to XG (SC: 0.026). FA loaded walls exhibited the highest WSI at the highest XG, due to the increased soluble polysaccharide chains and enhanced water dissolution. WAR remained high but lower than WSI, indicating hydroxyl and carboxylate group availability for hydrogen bonding between polymers and water molecules. Swelling capacity followed a similar trend to WAR but remained consistently low, confirming a stable system with controlled hydration properties suitable for encapsulation and controlled release of FA.

3.4 Encapsulation Efficiency

The encapsulation efficiencies were quantified using UV-Vis spectrophotometry. The results (Figure 5) showed a progressive increase in encapsulation efficiency (71.26% to 80.52%) with increasing XG concentrations, indicating that XG plays a critical role in enhancing FA entrapment. FABW4 showed the lowest EE 71.26%, that was lower than all XG-containing walls ($p < 0.05$). Improved encapsulation noticed in XG-containing walls may be associated with the increased viscosity provided by XG, which could enhance the wall density and promote greater retention of FA. The data demonstrated that even minimal XG (0.01–0.02g) significantly improves EE compared to HPMC alone, while the highest XG amount (0.05g) provides maximum EE. Additionally, encapsulation is influenced by physicochemical properties of the actives and encapsulating agents, including water solubility, molecular size/weight, and sensitivity.[15] Higher EE in XG-containing systems may be associated with intermolecular interactions between the anionic carboxyl groups of XG and the phenolic hydroxyl groups of FA, as observed by the spectral changes in FTIR. These findings are consistent with some studies showing polysaccharide-based encapsulation systems with higher carboxyl groups achieve improved EE for phenolics, compared to single-polymers, thereby confirming HPMC-XG biopolymeric walls as an optimal delivery carrier for FA.[16]

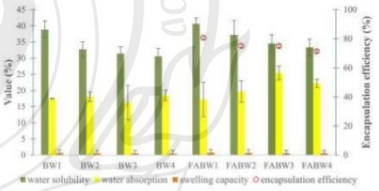

Figure 5. Physicochemical properties and encapsulation efficiencies of BW and FABW.

FA loaded walls, particularly the system containing highest XG amount (0.05g), appeared

to represent an optimal ratio, providing greater characterization result, favorable physicochemical properties, and highest encapsulation efficiency for FA. Thus, further assessment of these encapsulated particles in terms of *in vitro* release, long-term stability and safety are strongly encouraged.

4. Conclusion

The absence of clearly visible pores in SEM images when FA was loaded suggests that FA may be distributed within the polymer walls rather than remaining as distinct surface crystals. This change is supported by the relatively high encapsulation efficiency, where BW1, exhibiting the largest initial pore size (51.49 µm), achieved the highest EE (80.52%), indicating that higher porosity may facilitate FA retention, whereas lower porosity may limit available space, to effectively retain FA. The statistical findings ($p<0.05$) confirm that XG is greatly important for optimizing EE in HPMC-XG biopolymeric walls.

Acknowledgements

The authors would like to express their gratitude to Mae Fah Luang University for providing facilities and financial support.

References

1. Purushothaman, J. R.; Rizwanullah, Md. Ferulic Acid: *A Comprehensive Review. Cureus*. 2024, *16* (8), 1-15.
2. Pueknang, J.; Saewan, N. *Molecules.* 2022, *27* (11), 1-19.
3. Rojas, K.; Verdugo-Molinares, M. G.; Vallejo-Cardona, A. A. *Food Chem. Adv.* 2024, *4,* 1-11.
4. Jiang, M.; Zhang, Y. *J. Agric. Food Res.* 2023, *11*, 1-6.
5. Mughal, M. A.; Iqbal, Z.; Neau, S. H. *AAPS PharmSciTech.* 2011, *12* (1), 77-87.
6. Yu, J. Y.; Roh, S. H.; Park, H. J. *Food Hydrocoll.* 2021, *111*, 1-8.
7. Jang, Y.; Koh, E. *Food Chem.* 2023, *405*, 1-9.
8. Vashisth, P.; Sharma, M.; Nikhil, K.; Singh, H.; Panwar, R.; Pruthi, P. A.; Pruthi, V. *Biotech.* 2015, *5* (3), 303-315.
9. Navarro-Flores, M. J.; Ventura-Canseco, L. M. C.; Meza-Gordillo, R.; Ayora-Talavera, T. del R.; Abud-Archila, M. *J. Food Sci. Technol.* 2020, *57* (11), 4111–4122.
10. Wan, S.; Dai, C.; Bai, Y.; Xie, W.; Guan, T.; Sun, H.; Wang, B. *ACS. Omega.* 2021, *6* (43), 28598-28610.
11. Sethi, S.; Saruchi; Kaith, B. S.; Kaur, M.; Sharma, N.; Kumar, V. *Cellulose.* 2020, *27* (8), 4565- 4589.
12. Wang, J.; Cao, Y.; Sun, B.; Wang, C. *Food Chem.* 2011, *124* (3), 1069–1075. Suksaeree, J.; Monton, C.; Madaka, F.; Chusut, T.; Saingam, W.; Pichayakorn, W.; Boonme, P. *AAPS. PharmSciTech.* 2014, *16* (1), 171-181.
13. Akhavan Mahdavi, S.; Jafari, S. M.; Assadpoor, E.; Dehnad, D. *Int. J. Biol. Macromol.* 2016, *85*, 379–385.
14. Fara, D. A.; Dadou, S. M.; Rashid, I.; Al-Obeidi, R.; Antonijevic, M. D.; Chowdhry, B. Z.; Badwan, A. *Pharmaceutics.* 2019, *11* (11), 1–24.
15. Gao, R.; Zhao, D.; Zhou, X.; Wan, Z.; Wang, X.; Rao, H.; Liu, X.; Gao, X.; Hao, J. *Curr. Res. Food. Sci.* 2025, *11*, 1–17.

CURRICULUM VITAE

NAME Zaw Myo Htet

EDUCATIONAL BACKGROUND

2018 Bachelor of Science (Honours)
Industrial Chemistry
University of Mandalay

SCHOLARSHIP

2024 European Union Mobility Programme for Myanmar (EMPM)

PUBLICATION

Htet, Z. M., & Lourith, N. (2026). Fabrication of biopolymeric walls for ferulic acid encapsulation. In *Proceedings of the Pure and Applied Chemistry International Conference 2026 (PACCON 2026)* (pp. 450–454). Mae Fah Luang University.